A Geothermal Heatpipe Prototype

Peter Zijm
December 2018

A geothermal heatpipe prototype

By

Peter Zijm

To obtain the degree of Master of Science

At the Delft University of Technology

Peter P. J. Zijm

PeterZijm@gmail.com

Student number: 4035658

Thesis committee

Prof. Dr. R. Delfos,	TU Delft, supervisor	
R.Delfos@TuDelft.nl		
Prof. Dr. Ir. B.J. Boersma	TU Delft, supervisor	
B.J.Boersma@TuDelft.nl		
To be announced.	TU Delft, independent.	
Ir P. S. Omrani	TNO	
Pejman.ShoeibiOmrani@TNO.nl		
Dr. ir. A. Twerda	TNO	
Aris.Twerda@TNO.nl		

A geothermal heatpipe prototype – Peter Zijm – Mechanical Engineering Master Thesis 2018

Preface

I am originally from the small island Texel in the north of the Netherlands. I am an adventurous and sportive young engineer with a compelling drive to understand the way things work. From a young age, I have always been interested in how the world around us moves and functions.

First and foremost I would like to thank my parents for their support that made both this thesis and the amazing time I had at university possible. I would like to express gratitude to my professors René Delfos and Bendiks Jan Boersma for their time and guidance on this Thesis. I would like to thank Pejman Shoeibi Omrani and Aris Twerda from TNO for a great internship that developed towards this thesis and their guidance and cooperation. Bart Hoek for the conversations and questions that kept me thinking about the set-up. In addition, the guys from DEMO, Jasper Ruigrok from the fluid mechanics workshop and the student workshop for the support in building the prototype.

Peter Zijm.
Delft,
January 2019.

Nomenclature

Parameter	Description	Units		Subscripts	
A	Area	m^2		a	Adiabatic
				c	Condenser
ϕ_2	Thermosiphon figure of merit	$\dfrac{kg}{K^{\frac{3}{4}} * s^{\frac{5}{2}}}$		e	Evaporator
				f	Film
T	Temperature	K		l	Liquid
				fg	Liquid to gas
p	Pressure	Pa		o	Outside
$\dot{Q}$	Heat	W		i	Inside
				p	Pool
l	Length	m		v	Vapour
				w	Wall
h	Enthalpy	$J * kg^{-1}$		hp	Heatpipe
FR	Fill ratio	-			
V	Volume	m^3			
D	Diameter	m			
ρ	Density	$\dfrac{kg}{m^3}$			
μ	Dynamic viscosity	$\dfrac{N * s}{m^2}$			
σ	surface tension	$N * m^{-1}$			
β	angle	$^\circ$			
S	Surface	m^2			
R	Resistance	$K * W^{-1}$			
g	Gravitational acceleration	$m * S^{-2}$			
k	Thermal conductivity	$\dfrac{W}{m * K}$			
c_p	Coefficient of pressure	$\dfrac{J}{kg * K}$			
α	Heat transfer coefficient	$\dfrac{W}{m^2 * K}$			
c	Speed of sound	$m * s^{-1}$			
m	Mass flow	$kg * s^{-1}$			
G	Mass flux	$\dfrac{kg}{m^2 * s}$			

Dimensionless numbers

Parameter	Description	Definition	Ratio
Re	Reynolds number	$\dfrac{\rho * v * D}{\mu}$	$\dfrac{inertia\ forces}{viscous\ forces}$
$Bo, E\ddot{o}$	Bond or Eötvos number	$D\left[\dfrac{g(\rho_l - \rho_v)}{\sigma}\right]^{0.5}$	$\dfrac{gravitational\ forces}{surface\ tension\ forces}$
Nu	Nusselt number	$\dfrac{\alpha_c * D}{k_l}$	$\dfrac{convective\ heat\ transfer}{conductive\ heat\ transfer}$
Pr	Prandtl Number	$\dfrac{\mu * c_{p,l}}{k_l}$	$\dfrac{viscous\ diffusion\ rate}{thermal\ diffusion\ rate}$
St	Stanton Number	$\dfrac{\alpha}{c_{p,l} * G} = \dfrac{h_{fg}}{c_{p,l} * \Delta T}$	$\dfrac{heat\ transfer\ rate}{thermal\ capacity}$
Kp	Pressure parameter	$\dfrac{p_v}{[g(\rho_l - \rho_v) * \sigma]^{0.5}}$	
C_1	Constant	$\dfrac{1}{4} * \left(\dfrac{3}{\pi}\right)^{\frac{4}{3}}$	
f_1	Function of bond number	Page 25 reference 7	
f_2	Function of Kp	Page 25 reference 7	
f_3	Function of angle β	Page 17 reference 7	

Acronyms

TU Delft	Delft University of Technology
TNO	Toegepast Natuurwetenschappelijk Onderzoek – Applied Science Institute
CBS	Statistics Netherlands – Dutch Government Statistic Agency
TPT	Two Phase Thermosiphon
FOM	Figure of Merit
NIST	National Institute of Standards and Technology
MATLAB	Matrix Laboratory – a multi-paradigm numerical computing environment

A geothermal heatpipe prototype – Peter Zijm – Mechanical Engineering Master Thesis 2018

Abstract

Heatpipes are promising devices for geothermal energy extraction owing to their effectiveness to transport heat. The goal of this research is to validate an analytical heatpipe model with experiments and to investigate the difficulties in designing and constructing geothermal heatpipes. There is a lack of literature and research concerning the operation, performance limits and construction of heatpipes suitable for geothermal heat extraction.

A prototype heatpipe is designed based on specifications for geothermal energy extraction and constructed in a laboratory set-up with sensors and data acquisition. The prototype set-up collects experimental data and is used to evaluate important parameters, requirements and practical design difficulties. This research shows the difficulties in designing a geothermal heatpipe taking into account fluid choice and physical limitations as well as complications in constructing a properly sealed heatpipe under the influence of repeated heating and cooling. Furthermore it shows the limitations of the analytical model by comparing the model predictions with experimental data.

A geothermal heatpipe prototype – Peter Zijm – Mechanical Engineering Master Thesis 2018

Table of Contents

A geothermal heatpipe prototype – Peter Zijm – Mechanical Engineering Master Thesis 2018

A geothermal heatpipe prototype – Peter Zijm – Mechanical Engineering Master Thesis 2018

1. Introduction

1.1 Research Goal

In a cooperation between the TU Delft and TNO, the reuse of gas and oil boreholes for heating and electricity production was investigated in the end of 2017 by P. Zijm [22]. Mathematical models were built and integrated into a program to predict the performance of direct heat extraction methods as well as a geothermal heatpipe.

This investigation concluded that due to a lack of literature and research concerning the operation, performance limits and construction of heatpipes suitable for geothermal heat extraction the current model required validation from experimental data. Current research is limited to heatpipes ranging from several meters length used for thermal permafrost stabilization down to heatpipes used for cooling in semiconductor industry of a millimetre length scale [5].

The effectiveness of heatpipes to transport heat make it a promising device for geothermal applications. To properly design for geothermal application research and experiments into the operation of heatpipes with lengths of hundredths' of meters up the kilometre length scale is required. This thesis presents experiments investigating the operation of such devices.

A prototype heatpipe is designed based on specifications for geothermal energy extraction and constructed as a laboratory set-up with sensors and data acquisition. The prototype set-up collects experimental data and is used to evaluate important parameters, requirements and practical design difficulties. The ultimate goal of this research is to validate the heatpipe model with experimental data, investigate the limitations of the analytical model and to explore the difficulties in designing and building geothermal heatpipes.
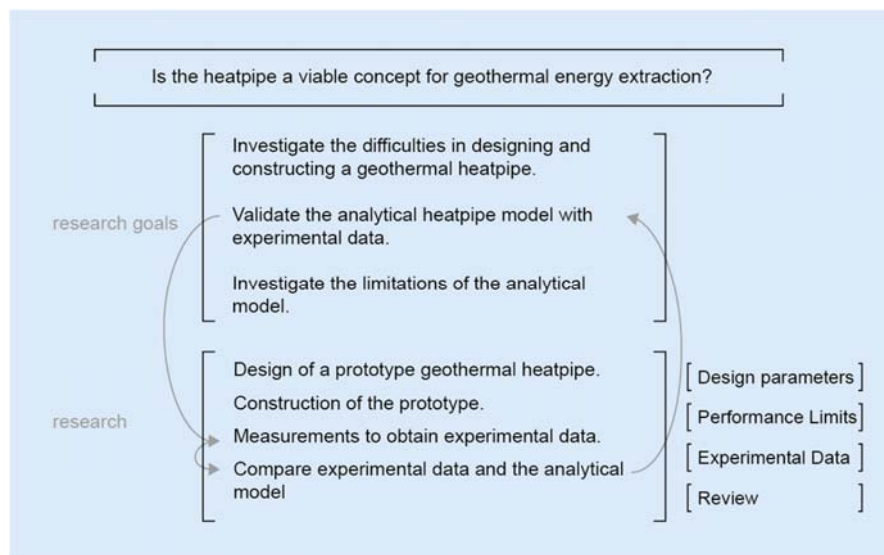

Figure 1: Research Plan

1.2   Project introduction

One of the main advantages of geothermal energy compared to solar and wind energy production is the constant availability. Geothermal energy is a prime candidate to supply heating, as it requires no energy conversion steps. According to the CBS, the Dutch governmental statistics agency, about 50% of energy consumption, after energy losses, is used for heating in the Netherlands [CBS Monitoring warmte 2015].

The technologies that make use of geothermal heat are either open or closed systems. The most common closed systems are heat pump based. These systems generally operate at shallow depths and supply heating for buildings.
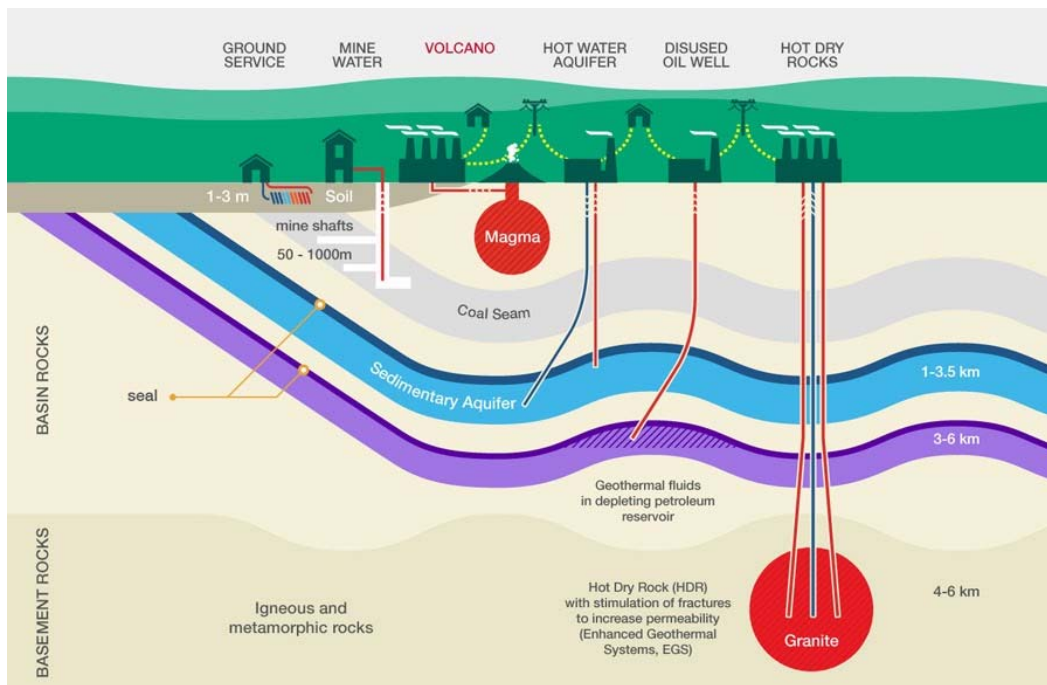

Figure 2: Geothermal energy systems. [12]

Open systems directly extract the hot geothermal fluid from warm layers in the earth. There are two main disadvantages to the direct extraction of geothermal fluid. The first is that extracting fluid in excess of the aquifer replenishment by underground water systems will reduce the water level and impede the heat extraction as happened in the Rotorua Geothermal Field in New Zealand. Here the natural geysers started disappearing due to lowering water level. Since intervention and an enforced bore closure program started in 1986, the geothermal field has been slowly recovering. The second disadvantage is that the geothermal fluid might require costly treatment before disposal or reuse as it can have high mineral content.

The term geothermal fluid refers to geothermal water, steam and gas separately or together depending on the temperature and pressure. The dissolved minerals, silica and salts are practically only found in the liquid phase. There are also non-condensable gases in the geothermal fluid, mainly carbon dioxide.

1.3 History

The first mention of a heatpipe type device was in 1944 by Gaugler [1]. Gaugler patented a lightweight heat transfer device that was essentially a very basic heatpipe. During that time there was little need nor attention for the passive heat transfer concept. The device was hardly cited until 1964 when George Groves [4] and his co-worker at the Los Alamos National Laboratory independently reinvented the same concept for the existing space program. Groves is the one who named this heat transfer device a heatpipe and advanced its applications. In the early days of space flight, NASA solved a major problem by teaming with Los Alamos Scientific Laboratory in development of the heatpipe. The problem was that the Sun-facing surfaces of a non-rotating satellite became very hot while surfaces not exposed to the Sun became extremely cold, a temperature differential that threatened failure of electronic systems. The solution, used in virtually all spacecraft since its development, is the heatpipe. A tubular device in which a working fluid alternately evaporates and condenses, transferring heat from one region of the tube to the other.

1.4 Description of the heatpipe

The heatpipe, shown in figure 3, is a heat-transferring device nowadays used in many applications. The heatpipe consists of a container with a working fluid inside it and has three main zones. An evaporator, adiabatic and condenser zone. At the evaporator, heat flows into the heatpipe and evaporates the working fluid. In the middle is an adiabatic section where heat transport occurs by vapour flow through the heatpipe. At the condenser zone, heat removal happens through condensation of the vapour.
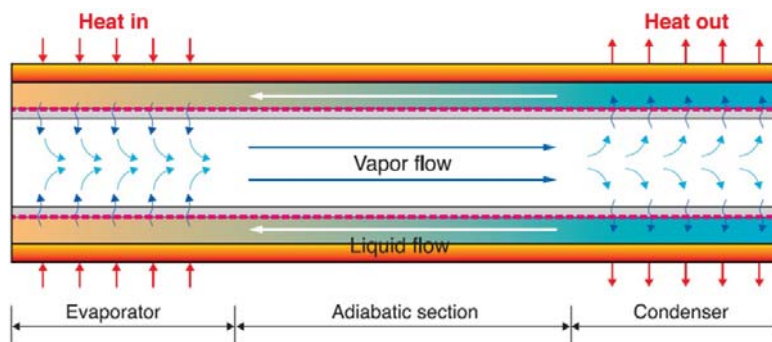

Figure 3: The Heatpipe. [15]

The two main properties that make a heatpipe an effective heat-transferring device is the effective heat transport capability at low temperature differences between the sink and the source [12] and the high energy content in evaporation.

To demonstrate the effectiveness of heat transport we can calculate the temperature difference that would be required to transport $1 \ kW$ through a solid copper tube. The Fourier equation for heat conduction is rearranged to give the temperature difference.

$$\dot{Q} = k * A * \frac{\Delta T}{\Delta x}$$

Equation 1: Fourier Heat Conduction

$$\Delta T = \frac{\dot{Q} * \Delta x}{k * A}$$

For a solid copper tube of $60\ mm$ diameter and $1\ m$ length, taking the conductivity of pure copper $k = 401\frac{W}{m*K}$ [18], the temperature difference required to transport $1\ kW$ of heat is approximately $900°C$. A heatpipe of the same size can transfer the same amount of heat with a temperature difference of less than $10°C$ [16]. What this example shows is that conduction of heat is not a suitable mechanism for transporting heat over lengths of a meter or more.

To show how much energy is required for evaporation we can compare the sensible and latent heat of water at atmospheric pressure. The latent heat of water, or energy required for evaporation, is approximately $2256\frac{kJ}{kg}$, [19]. The sensible heat, or energy used to increase the temperature, is about $4.2\ \frac{kJ}{kg*K}$, [19].

From the data, it follows that heating an amount of water from $0°C$ to $100°C$ requires approximately $420\frac{kJ}{kg}$, about five times less than evaporating the same amount.

1.5 Structure of the thesis

Chapter 2 explains the theoretical operation of heatpipes by looking at the working fluid and the limitations to heatpipe performance. This chapter concludes with a Case Study into the limits of the geothermal prototype heatpipe. Chapter 3 presents the prototype set-up design as well as the sensors and data acquisition capabilities. Chapter 4 describes the analytical MATLAB model in detail. In Chapter 5 the results from this research are reviewed and discussed. Chapters 6 and 7 contain the Appendixes and References respectively.

2. Heatpipe theory

2.1 Two phase vertical thermosiphon (TPT)

There are many types of heatpipes such as wicked, loop, rotating and pulsating devices as well as many options for shapes and configurations. For a comprehensive review of heatpipe types, the reader can consult Heatpipes: Review, Opportunities and Challenges by A. Faghri [5].

The theory in this chapter is limited to a vertical two-phase thermosiphon (TPT) as shown in figure 4. The TPT is sometimes referred to as a gravity driven heatpipe. This device consists of a simple, single closed tube without a wick.
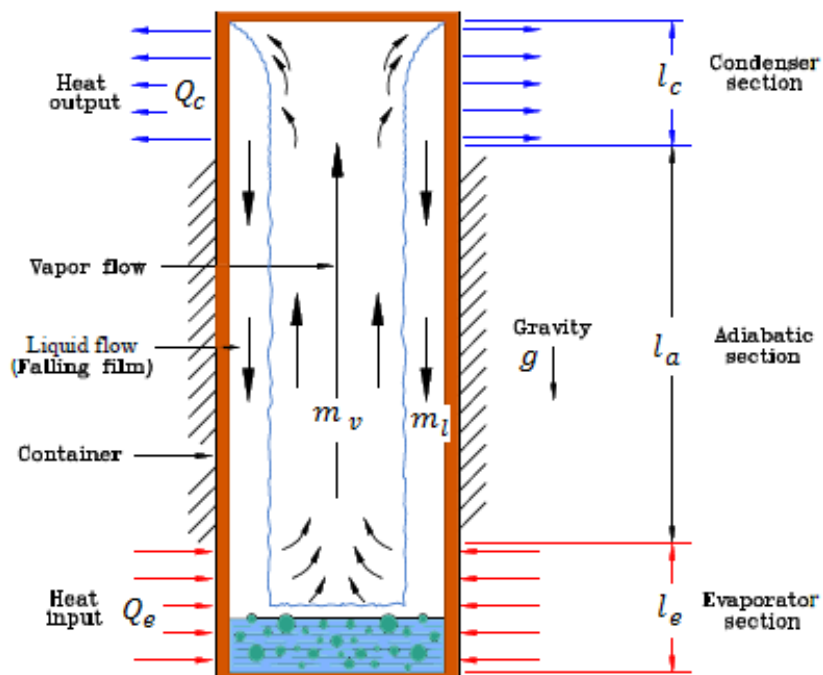

Figure 4: Two Phase Thermosyphon type Heatpipe [5].

2.2 Theoretical operation

In all heatpipes, the working fluid has to recirculate when a temperature difference exists between the evaporator and the condenser. For the type of heatpipe considered in this research the working fluid recirculation is driven by gravity. Numerical and analytical simulation of heatpipes has progressed significantly in recent decades. Reports in literature are available for full three-dimensional incompressible numeric models for both transient and steady state [5] to investigate the complex flow phenomena within heatpipes. The theory in this report will be limited to an incompressible heatpipe model that can be used as a design tool.

The assumption of an incompressible working fluid is an acceptable assumption when the flow velocity v is small compared to the velocity of sound c, i.e. the $Mach$ number. According to Kundu [13] in engineering practice this corresponds to a $Mach$ number smaller than 0.3.

$$Ma = \frac{v}{c} < 0.3$$

2.2.1   Working fluid

Two groups of fluid properties called figures of merit are commonly used indicators of the relative effectiveness of different working fluids. The figure of merit ϕ_1 applies to capillary heatpipes and the figure of merit ϕ_2 applies to two-phase thermosiphons. ϕ_2 is a measure of properties of the fluid that aid heat transfer. Whilst the figure of merit is a useful guide, it is not the sole criteria and ignores other important factors such as material compatibility and vapour pressure.

It is expected that the temperature drop over a thermosiphon is dominating the heatpipe performance [7]. ϕ_2 is defined such that the maximum value corresponds to a minimum in temperature drop. The Figure of Merit ϕ_2 is derived from an analysis of the condenser thermal resistance under the assumptions of film condensation, negligibly small pressure drop in the vapour and negligibly small shear forces between the counter-current flows of liquid and vapour.

It is important to note that the assumption of a negligibly small pressure drop in the vapour may not be accurate for long geothermal heatpipes due to hydrostatic head and should be re-evaluated at a later stage.

The figure of merit for thermosiphons [7] is defined by the latent heat h_{fg}. The thermal conductivity of the liquid k_l. The density of the liquid ρ_l and the viscosity of the liquid μ_l as:

Figure of merit: $\phi_2 = \left(\dfrac{h_{fg} * k_l^3 * \rho_l^2}{\mu_l} \right)^{\frac{1}{4}}$

In figure 5 the figure of merit for several fluids are plotted as a function of temperature.
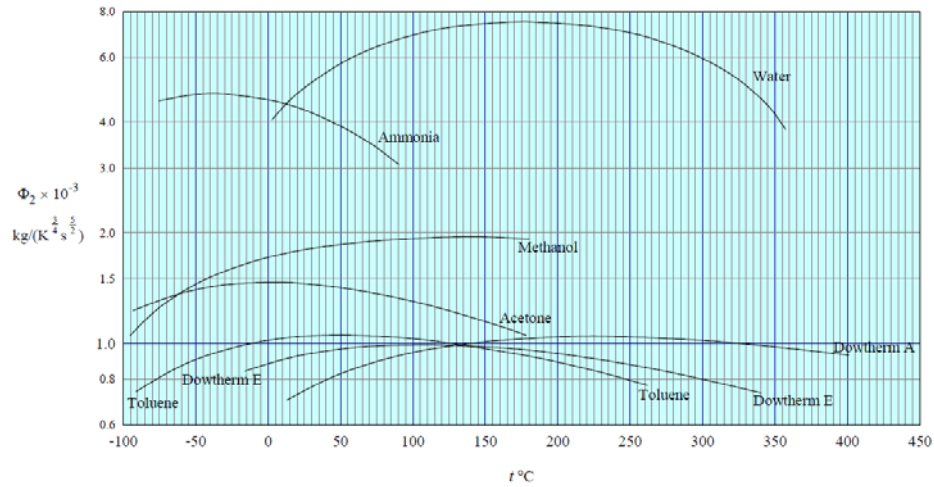
Figure 5: Figure of Merit as a function of Temperature [6]

Figure 6 shows the vapour pressure as function of temperature for several fluids. It shows that the vapour pressure for most fluids increases exponentially with temperature. The vapour pressure dictates the proposed temperature operating range for a fluid.
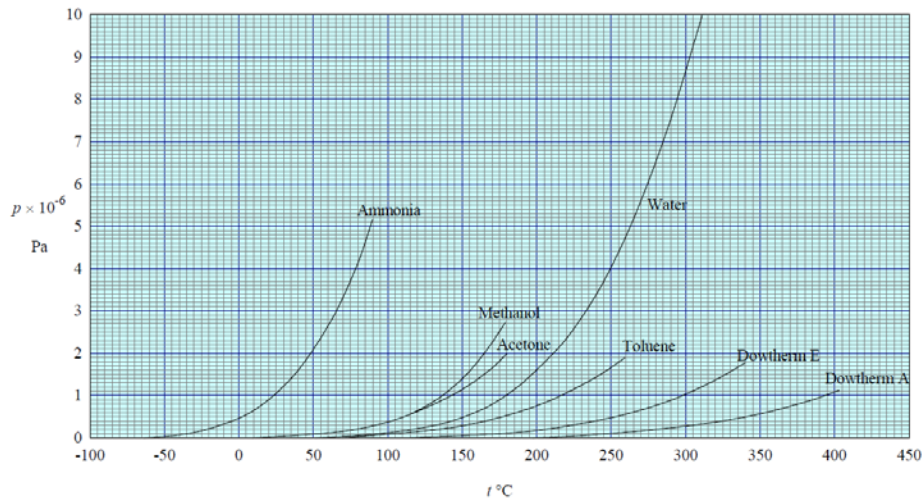

Figure 6: Vapour pressure as a function of temperature [6]

Common fluids and their proposed operating temperature ranges are given in appendix 6.3.1. As a rule of thumb, the useful temperature range for theses fluids extends from a minimum vapour pressure of $0.1\ bar$ to a maximum of $20\ bar$. Below $0.1\ bar$ the low vapour pressure is expected to limit heat flow. Above 20 bar the performance of the heatpipe is most likely limited due to the conduction resistance of the container wall.

Furthermore the liquid should be compatible with the container materials. Appendix 6.3.2 contains an overview with fluid compatibility for several common container materials.

15

2.3 Limitations to heatpipe performance

Several mechanisms limit the performance of heatpipes. As the temperature difference across a heat pipe or thermosiphon is increased the overall rate of heat transfer increases until a maximum is reached. This may be due to a boiling crisis, an excessive pressure drop in the vapour or due to a failure in the supply of liquid to the heated surface.

Figure 7, from the book Heat Pipes Theory Design and Applications [2], gives a representation of the different limits as a function of the operating temperature. Not all limits result in a failure of the operation of the heat pipe. Some of the limits are most notable during the start-up period leading up to steady operation. In this chapter the limits shown in figure 7 are explained.
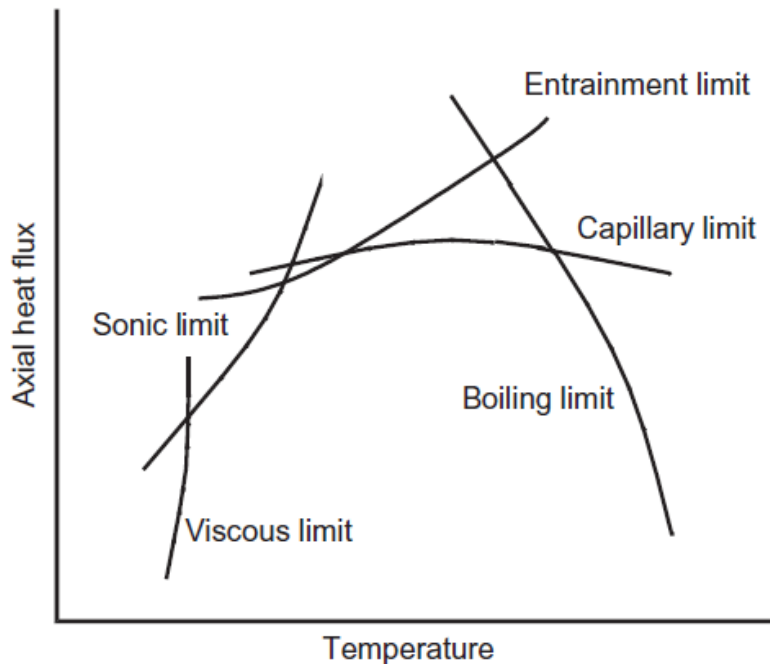

Figure 7: Heatpipe Performance Limits. [2]

2.3.1   Viscous limit

When operating a heatpipe at the bottom end of the operational temperature range the vapour pressure can limit the heat flow. The minimum vapour pressure, which occurs at the closed end of the condenser, can be very small. The pressure drop Δp_v in the vapour duct is then constrained by the low vapour pressure at the closed end of the evaporator and the effectively zero pressure at the condenser end. Since Δp_v increases with the heat transfer rate $\dot{Q}$, the constraint on Δp_v limits the heat flow $\dot{Q}$.

Equation 2 gives the maximum heat flow $\dot{Q}_{max}$. In this equation A_v is the vapour duct area and D_{Ev} is the equivalent diameter for the vapour flow area.

$$\dot{Q}_{max} = \frac{A_v * D_{Ev}^2 * h_{fg} * p_v * \rho_v}{64\mu_v * l_{eff}}$$

Where the effective length $l_{eff} = \frac{l_e}{2} + l_a + \frac{l_c}{2}$. See figure 4.

The viscous limit is also referred to as the vapour pressure limit.

2.3.2 Sonic limit

At low operating pressures, the vapour velocity may be appreciable compared to the velocity of sound in the vapour for the given fluid. If the local speed of sound equals the vapour velocity the flow will be chocked and as a result limit the maximum heat flow.

Equation 3 gives the maximum axial vapour mass flux in $\frac{kg}{s*m^2}$:

$$\frac{\dot{Q}_{max}}{A * L} = 0.5 * (p_v * \rho_v)^{0.5}$$

2.3.3 Dry-out limit

The gravity driven heatpipe requires sufficient liquid to cover the entire evaporator wall during operation with a film of liquid. Insufficient working fluid will result in dry patches in the heatpipe that limit the performance. In literature, only empirical data is available for filling ratios of the heatpipe. ESDU 80017 [6] gives two basic formula for a rough estimate:

1. The fill ratio FR should be more than 50% where the fill ratio is defined as the total volume V_l devided by the evaporator volume $A_{axial} * l_e$:

$$FR = \frac{V_{hp}}{A * l_e} \text{ and } V_{hp} \geq 0.001 \, D * (l_e + l_a + l_c)$$

Though there is no upper limit given, a surplus of liquid will reduce the effectiveness of the heatpipe [10].

2.3.4 Entrainment limit

The entrainment limit, sometimes called the counter-current flow limit, occurs when the rate of entrainment of liquid by the vapour prevents downward flow of the liquid. Equation 4 gives the maximum heat transfer due to the entrainment limit. σ_l is the surface tension of the liquid.

$$\frac{\dot{Q}_{max}}{A * L} = f_1 * f_2 * f_3 * \rho^{0.5} * [g(\rho_l - \rho_v) * \sigma_l]^{0.25}$$

The parameters f_i are given in ESDU 81038 [6]. f_1 is a function of the Bond number.

$$Bo = D\left[\frac{g(\rho_l - \rho_v)}{\sigma}\right]^{0.5}$$

f_2 Is a function of the dimensionless parameter K_p defined as:

$$K_p = \frac{p_v}{[g(\rho_l - \rho_v) * \sigma]^{0.5}}$$

$$f_2 = K_p^{-0.17} \: for \: Kp \leq 4 * 10^4$$

$$f_2 = 0.165 \: for \: Kp > 4 * 10^4$$

The parameter f_3 is a function of the Bond number and dependent on the inclination angle β. For a vertical heatpipe f_3 it is equal to 1.

2.3.5 Boiling limit

The boiling limit is associated with the film-boiling region where the heat flux is significantly limited. This phenomena occurs when a stable film of vapour forms between the liquid and the heated wall. Figure 8 gives the general pool-boiling curve for water at atmospheric pressure. The heat flux reaches a maximum at the end of the nucleate boiling region after which a very steep decline in maximum heat flux occurs. In practice, this results in a sudden increase in the wall temperature that is generally unwanted and potentially dangerous in engineering systems.
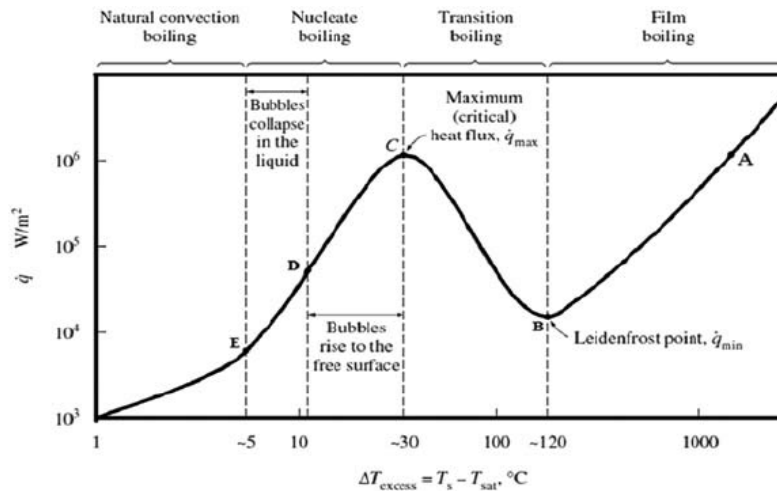

Figure 8: Typical boiling curve of water at atmospheric pressure. [20]

Equation 5 gives the maximum heat flow for pool boiling:

$$\frac{\dot{Q}_{max}}{S_e} = 0.12 * h_{fg} * p_v^{0.5} * [g(\rho_l - \rho_v)\sigma_l]^{0.25}$$

Equation 5: Boiling limit

In equation 5, S_e is the surface of the evaporator. In flow boiling, as opposed to pool boiling, the magnitude of the maximum heat flux is expected to be similar provided there is no dry out.

2.3.6   Maximum heat transfer

The maximum heat transfer is limited to the lowest value of the heatpipe limits. It is however not recommended to design for this exact limit. The reason is that these limits are engineering estimates based on several assumptions and in many cases not that accurate. According to ESDU 81007 it is recommended engineering practice that thermosiphons are designed to operate at less than 50% of the maximum heat flux.

2.4 Case Study: Limits of a prototype geothermal heatpipe.

2.3.1 Introduction

This paragraph consists of a case study into the limits of a prototype heatpipe. The goal of the study is to evaluate design choices for a geothermal heatpipe prototype. Fluid properties as a function of temperature are obtained from the National Institute of Standards and Technology Refprop database [21]. The limits are evaluated as a function of the operating temperature and heatpipe diameter. The required heating power for a geothermal heatpipe is set at 10 kW. Therefore, the lower limit of the theoretical expected heat flow is set at 20 kW as explained in 2.4.6.

2.3.2 Variables

Several tube diameter for readily available tube sizes that are suitable for a geothermal heatpipe are considered. Borehole dimensions limit the maximum diameter. The operating temperature range depends on the working fluid and is limited by the heatpipe container material.

2.3.3 Results

Figures 9 and 10 give the maximum heat flow for the viscous and sonic limits as a function of operating temperature and diameter.
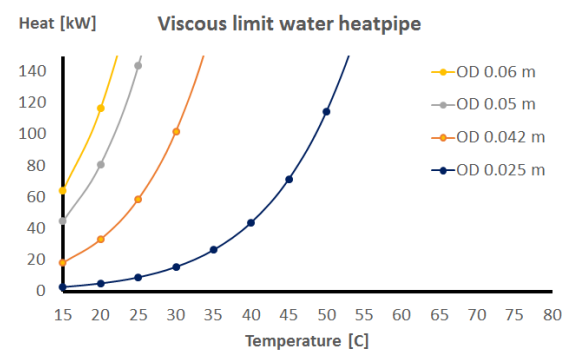

Figure 9: Viscous Limit of a Water Heatpipe.
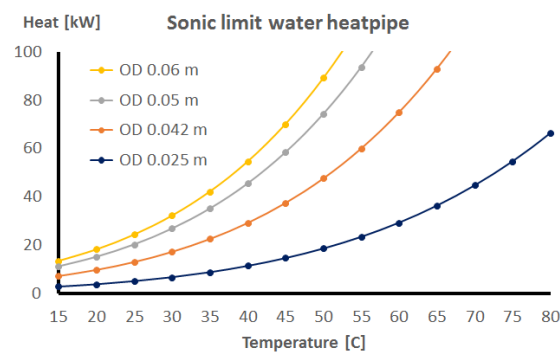
Figure 10: Sonic Limit of a Water Heatpipe.

The environment temperature is approximately $20°C$ and the viscous and sonic limits will play a role during start-up of the heatpipe. The steady operating temperature range of the heatpipe is $40°C$ to $60°C$ and thus the limits at low temperature are of little consequence since they do not prevent heating of the working fluid. For the sonic limit, the smallest diameter of 0.025 m at 40 degrees Celsius is below the limit and thus this diameter does not comply with the heat flow requirement.

Figures 11 and 12 show the maximum heat flow for the boiling and entrainment limit respectively

Figure 11: Boiling Limit Water Heatpipe. **Figure 12: Entrainment Limit Water Heatpipe.**

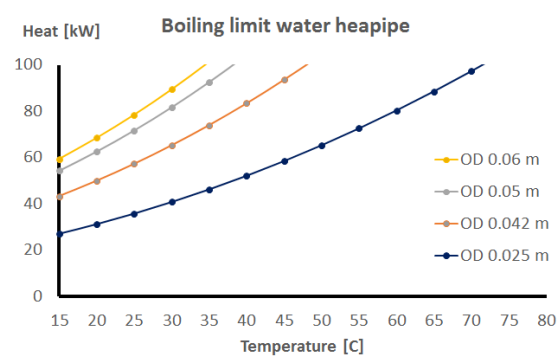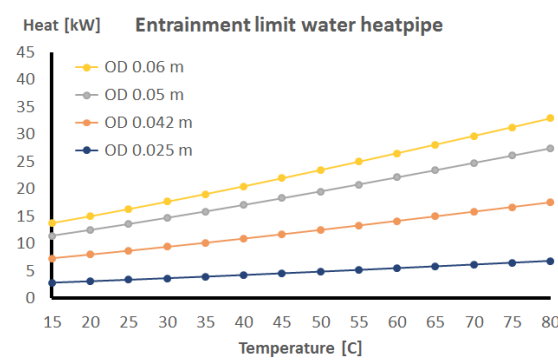Figure 11 shows that the Boiling limit is not limiting the heat flow at any operating temperature for the given diameters. Figure 12 shows that the entrainment limit of the heatpipe limits the performance depending on which diameter is used. It shows that only the two largest diameters are above the design limit for temperatures above $50°C$. For a $0.05\ m$ diameter tube operating below $50°C$ the entrainment limit is lower than the required 20 kW heat flow.

2.3.4   Conclusion & Discussion

From the results of the Case Study, it is concluded that the prototype heatpipe design choices are dictated by the entrainment limit. The three smallest diameters do not comply with the proposed heater capacity and subsequent minimum heat flow limit of $20\ kW$ for temperatures between $40°C$ to $60°C$.

The 0.06 m diameter tube is selected for the prototype design because the entrainment limit is not reached over the full operating temperature range. In figure 13 the limits for the 0.06 m OD tube are plotted to visualize the full operating space, highlighted in red, in terms of heat as function of the operating temperature.
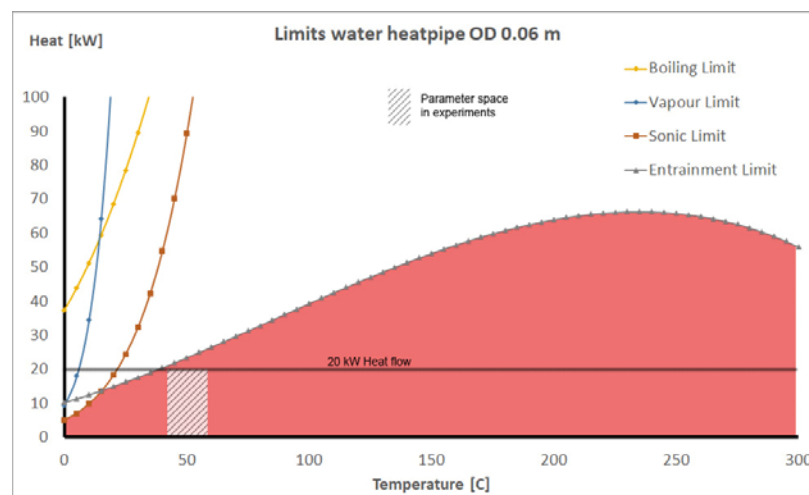

Figure 13: Limits for the 0.06 m OD Water Heatpipe

3 The heatpipe prototype

3.1 Design

Figure 14 shows a process and instrumentation diagram of the prototype heatpipe set-up. The fluid flow between components is indicated with red arrows.

The heatpipe is shown with the Band Heaters attached at the bottom evaporator section. Thermocouples for temperature measurement are locatod in and on the heatpipe and plate heat exchanger. The heat flow into the evaporator is measured at the band heaters using power indicators. The power fed to the bandheaters is controlled by a variable current transformer. The pressure sensor is located at the top of the heatpipe.

The plate heat exchanger is connected to an in-house coolant circuit. The flow of coolant from the coolant inlet is kept at a constant temperature of approximately $14°C$. Flow control is achieved using a rotameter in combination with a hand control valve. The pump is part of the recirculation bypass adding the possiblity to recirculate a portion of the heated coolant to increase the temperature at the heat exchanger inlet.

The vacuum pump is connected at the highest point of the heatpipe set-up with a hand valve to close the connection after air inside the set-up has been evacuated to the environment.
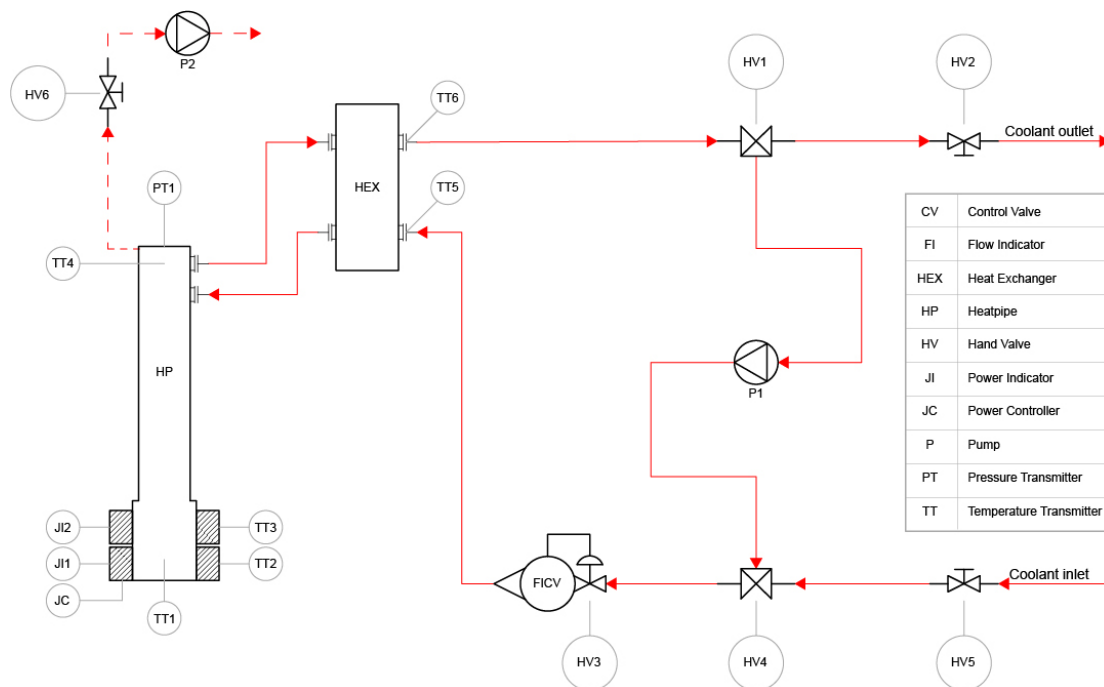

Figure 14: Process and Instrumentation Diagram Heatpipe Prototype Set-up (ISA-5.1-2009)

Figures 15 and 16 on the next pages give a side by side view of the prototype set-up and a SolidWorks model.

In figure 15 the plate heat exchanger is encased in an insulating box. The tube at the top that connects the pressure sensor to the heatpipe as well as to the vacuum pump is insulated and runs down the frame of the heatpipe. The red handle from the valve to close the connection to the vacuum pump is sticking out from behind the heatpipe.

The PVC T-piece is modified by glueing several connection tubes to the T-piece as well as a threaded o-ring connection. This is done to connect the heat exchanger inlet to the heatpipe as well as the pressure sensor and the vacuum pump. The vacuum pump is not visible in figure 15.

Figure 16 shows the adiabatic viewing section connected with a Plexiglas flange to the steel heatpipe evaporator tube. The vapour flow through the Plexiglas pipe is channelled to the plate heat exchanger where it condenses and is fed back to the adiabatic section through a condensate return tube. The band heaters are powered from the 230V AC building electrical system through a variable current transformer that regulates the power to the bandheaters.
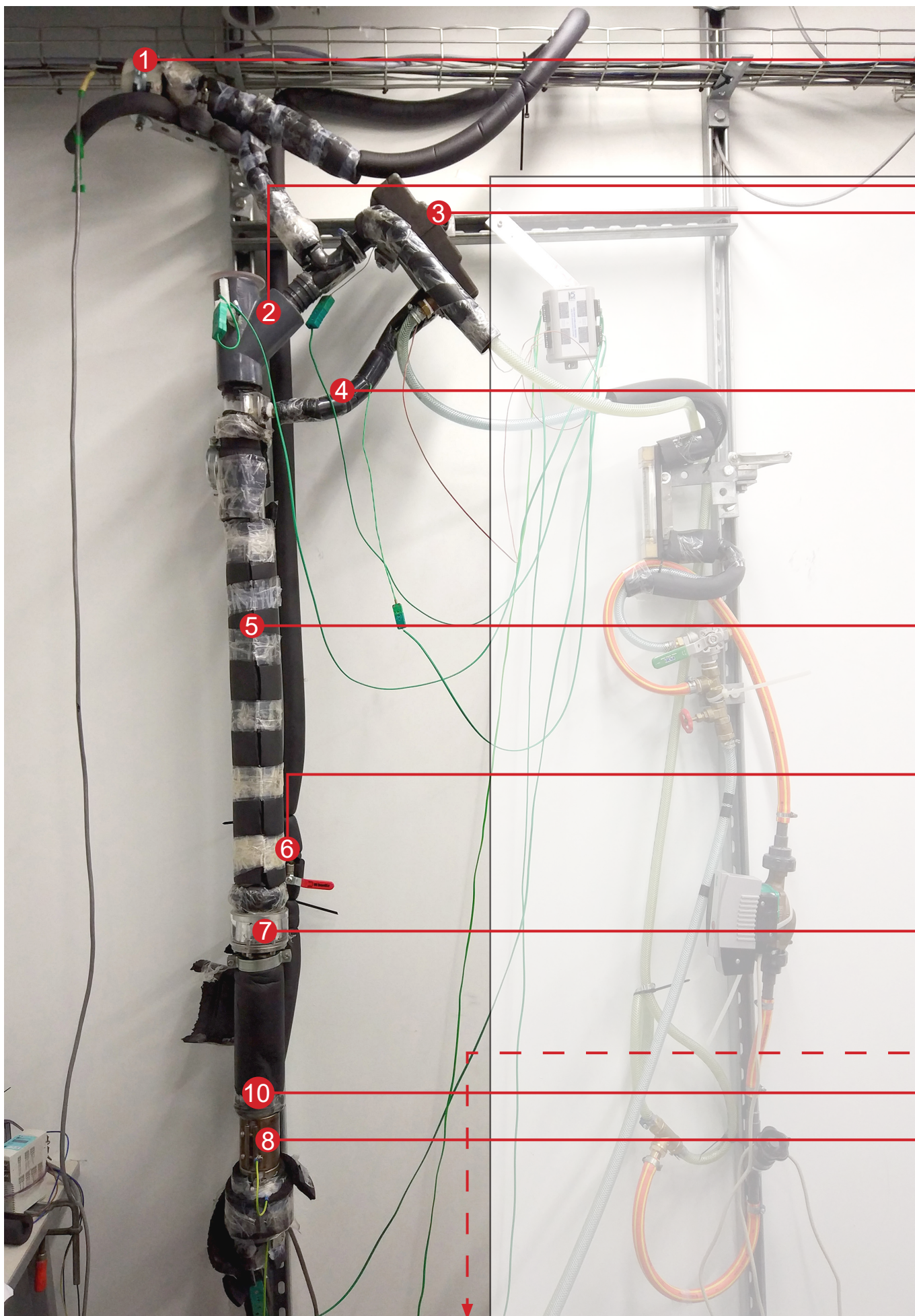
SOLIDWORKS HEATPIPE MODEL

1. Pressure sensor   PT1
2. PVC T-piece
3. Plate heat exchanger   HEX
4. Condensate return
5. Plexiglass tube
6. Ball valve   HV6
7. Plexiglass flange
8. Band heaters
9. Vacuum pump   P2
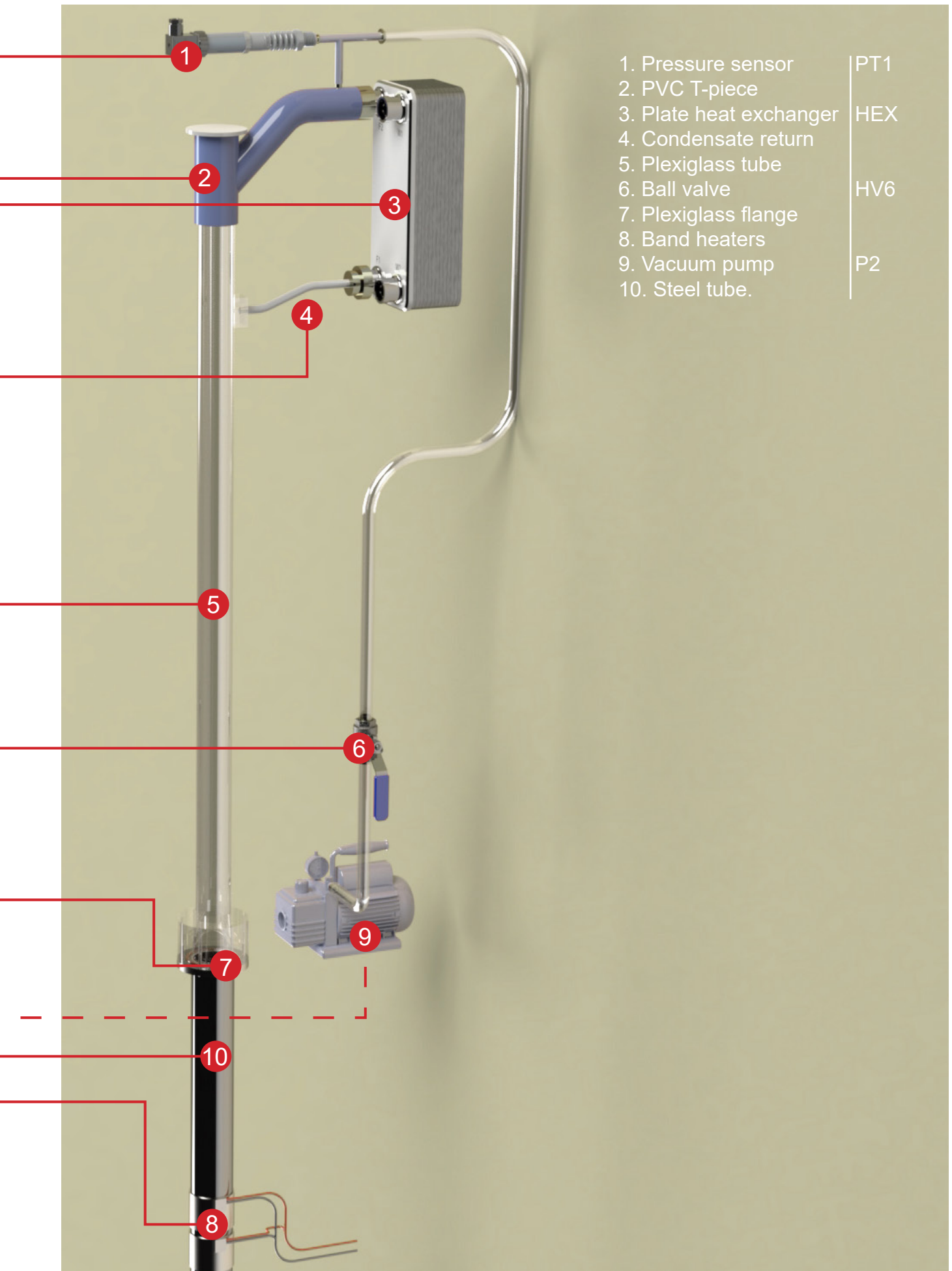10. Steel tube.

Figure 17 on page 28 shows the thermocouple measurement locations on the heatpipe set-up. Part of the insulation from the set-up has been removed in the picture. At the bottom of the prototype the top band heater is visible. The band heaters are directly clamped onto the heatpipe evaporator surface. This surface is polished and a thin layer of heat transfer paste is applied before attaching the heaters. Wires from the thermocouples in green and brown are connected to the Omega DAQ data acquisition device next to the set-up.

The temperature difference measured between the coolant at the plate heat exchanger outlet (TT6) and the coolant flowing to the inlet (TT5) is used to calculate the energy leaving the heatpipe set-up.

$$\dot{Q}_{Condenser} = \dot{m}_{Coolant} * c_{p,l} * (T_{Coolant_{Out}} - T_{Coolant_{In}})$$

The Temperature difference between the vapour temperature (TT4) and the average plate heat exchanger temperature, defined as the average temperature of the coolant (TT5 and TT6), is used to estimate the heat transfer resistance over the condenser side.

$$\bar{T}_{Coolant_{Average}} = \frac{T_{Coolant_{In}} + T_{Coolant_{Out}}}{2}$$

$$\bar{R}_{Condenser} = A * \frac{(T_{Vapour} - \bar{T}_{Coolant_{Average}})}{\dot{Q}}$$

The Temperature difference between the pool (TT1) and the average temperature of the bandheaters (TT2 and TT3) is used to estimate the heat transfer resistance over the evaporator side of the heatpipe.

$$\bar{T}_{heater_{average}} = \frac{T_{Heater_1} + T_{Heater_2}}{2}$$

$$\bar{R}_{Evaporator} = A * \frac{(\bar{T}_{Heater_{Average}} - T_{Pool})}{\dot{Q}_{Out}}$$

Figure 18 shows the coolant circuit of the heatpipe set-up.

The coolant circuit connected to the plate heat exchanger are the blue and green colored plastic tubes for the inlet and outlet respectively. The blue tube runs from the coolant inlet to the flow control hand valve (HV3) and then to the flowmeter (FM) and on to the plate heat exchanger. The green tube starts from the outlet of the plate heat exchanger and runs back to the coolant outlet. The orange and yellow colored plastic tubes are part of the bypass circuit. These tubes connect the inlet and the outlet of the bypass pump (P1) to the rest of the circuit .

THERMOCOUPLE MEASURMENT LOCATIONS
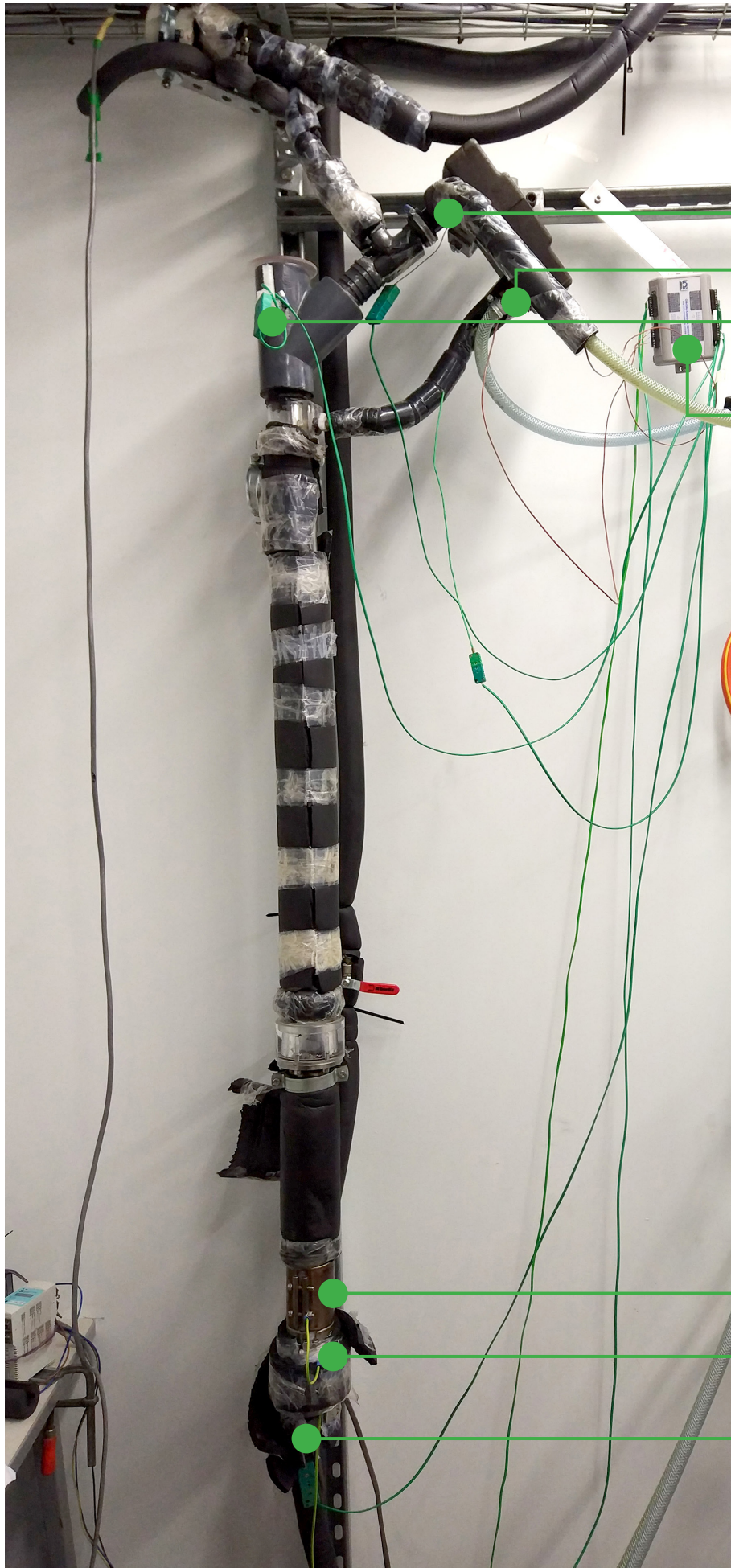
Coolant out (TT6)

Coolant in (TT5)

Vapour (TT4)

Omega Data Aquisition Device

Band heater 02 (TT3)

Band heater 01 (TT2)

Pool (TT1)

COOLANT FLOW CIRCUIT

CT Platon Flowmeter (FM)

Flow Control Hand Valve (HV3)

Bypass Pump (P1)

Coolant Outlet

Bypass Circuit Control Hand Valve (HV1)

Coolant Inlet

3.2 Sensors and data acquisition

3.2.1 Thermocouples

The temperatures in the heatpipe set-up are measured with NiCr-NiAl type K shielded thermocouples. These thermocouples have a specified accuracy of $\pm$ 1.5°C [29] over the range of -100°C to 250°C. Calibration of the thermocouples for 0 °C and 100°C is performed in ice water for 0°C and in boiling water for 100°C.
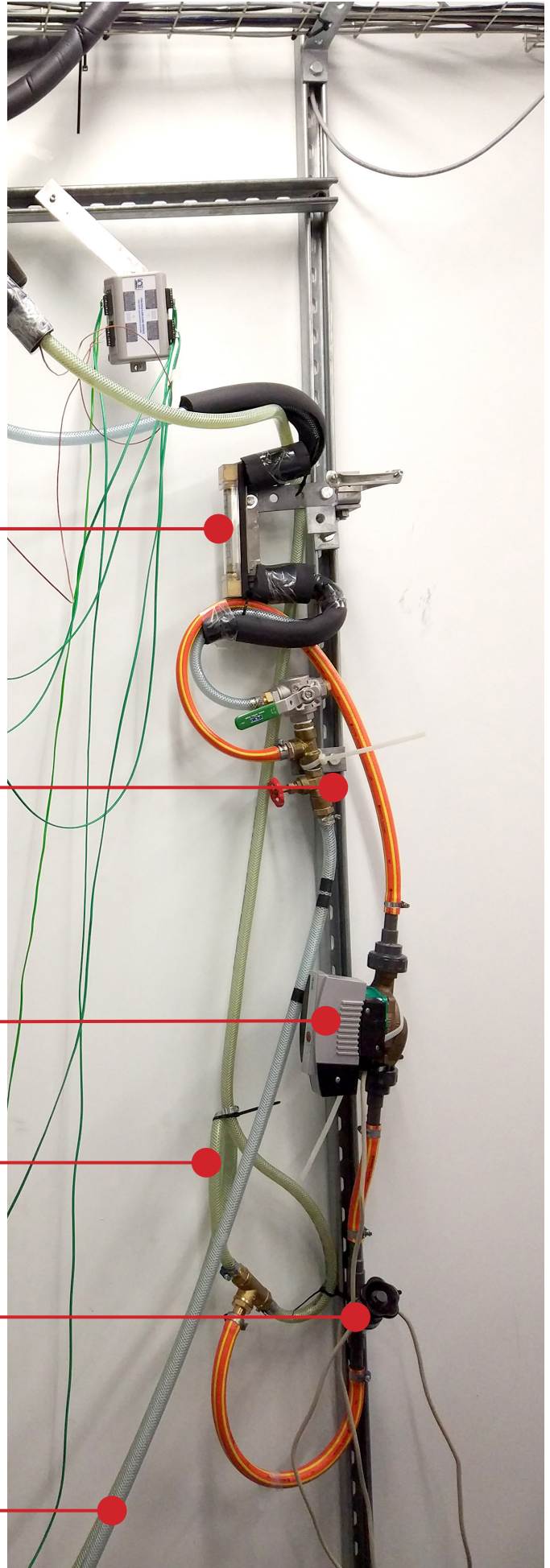
Data points	Thermocouple number	Average Temperature	Standard deviation
n	#	°C	$-$
50	1	100,24	0,049
50	2	99,79	0,050
50	3	99,70	0,211
50	4	100,16	0,109
50	5	100,73	0,031
50	6	100,93	0,058

Table 1: Thermocouple calibration data.

The calibration data in table 1 shows that the thermocouples are all within three standard deviations, or 99.7% confidence interval, of the specified accuracy. Similar results were obtained for calibration at 0 °C. Therefore the thermocouples are expected to be within the specified $\pm1.5°C$ accuracy within a $0°C\ to\ 100°C$ range.

3.2.2 Flow Rotameter

A rotameter with hand control valve measures the coolant mass flow in the coolant circuit. To calibrate the rotameter the amount of liquid over time is measured using a scale and timer. These measurements are repeated for 10 points on the rotameters scale in increments of 10 mm. The calibration curve in figure 19 is the result of a linear fit through the obtained data points.
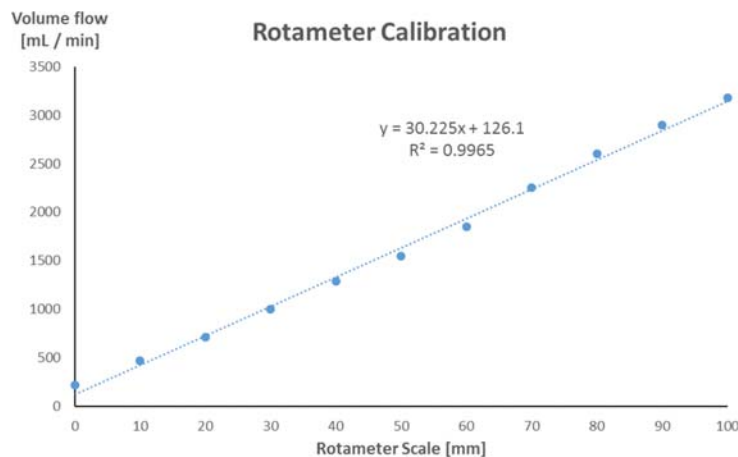

Figure 19: Rotameter calibration curve.

3.2.3   Heat flux sensors

To get a better understanding of the boiling process and local heat transfer inside a geothermal heatpipe heat flux sensors, shown in figure 20, were included in the prototype design.

During the testing phase, these heat flux sensors are attached between the band heaters and the outside of the evaporator tube. Heat transfer paste is used to facilitate heat conduction. However, adding the heat flux sensors resulted in an increase in heat transfer resistance from the band heaters to the working fluid.

Table 2 shows the resistance over the evaporator measured with and without the heat flux sensors. The resistance estimated from applying Fourier's heat conduction equation to the evaporator tube is included in table 2. The heat flux sensors used for testing are 600 micron thick and encapsulated in copper. Therefore, the added resistance should be small compared to the evaporator tube resistance.

Experiment with heat flux sensors	Experiment without heat flux sensors	Estimate from Fourier equation
$R_e \cong 0.1230 \frac{°C}{W}$	$R_e \cong 0.0210 \frac{°C}{W}$	$R_e \cong 0.0185 \frac{°C}{W}$

Table 2: Resistance over the evaporator tube.

Table 2 shows the resistance with heat flux sensors increased by nearly an order of magnitude on the evaporator side. This might be due to contact patches and possibly air pockets forming between the band heaters, heat flux sensors and evaporator tube.

The experiment without heat flux sensors shows a resistance which is close to the theoretical resistance of the stainless steel tube. The increase in resistance lead to heatpipe operating temperatures above what is allowable for Plexiglas at $2\,kW$ heat input. Therefore, the heat flux sensors are not included in the final set-up.

Figure 20: Heat flux sensors.

Figure 21: Omega DAQ data acquisition device.

3.2.4   Data acquisition device

To read and import thermocouple data an OMEGA DAQ data acquisition device, figure 21, is used. This device has 16 analogue signal inputs making it capable of reading up to eight differential thermocouples signals and has integrated cold junction compensation with a specified accuracy of $\pm 1°C$.

3.3 Measurement procedure

At the start of an experiment, the heatpipe fill ratio is set by adding the required amount of working fluid. Subsequently air is evacuated from the heatpipe with the vacuum pump. When the system pressure reaches the saturated vapour pressure, the valve to the vacuum pump is closed. The coolant mass flow is set with a regulating valve and the rotameter. Finally, the band heaters are set to the required power using the alternating current transformer and power indicators.

4 Theoretical model

4.1 Introduction

Modelling of a heat pipe is possible for various levels of detail depending on the requirements. Figure 22 gives an overview of the different variables, phenomena and governing equations that might be of interest when simulating heat pipe performance.

Heat source		Heat sink
Evaporator		Condenser

Heat conduction in heat pipe container

Variables	Phenomena	Governing equations
Temperature Heat input Heat output	Conjugate effects Radiation or convection B.C. 's Geometry effects	Heat conductions Stefan–Boltzmann law Fourier law

Liquid flow and heat transfer in wick structure

Variables	Phenomena	Governing equations
Temperature Velocity Pressure Gravity	Phase change Porous media flow Interfacial shear stress Liquid entrainment Boiling limitation	Continuity equation Modified Navier–Stokes equations Averaged energy equation

Liquid–vapor interface

Variables	Phenomena	Governing equations
Contact angles Interfacial curvature Interface position Interfacial mass fluxes	Capillary pressure Disjoining pressure Evaporation Condensation	Interfacial mass balance Interfacial species balance Interfacial momentum balance Interfacial energy balance Clapeyron or Kelvin equation

Vapor flow in heat pipe core

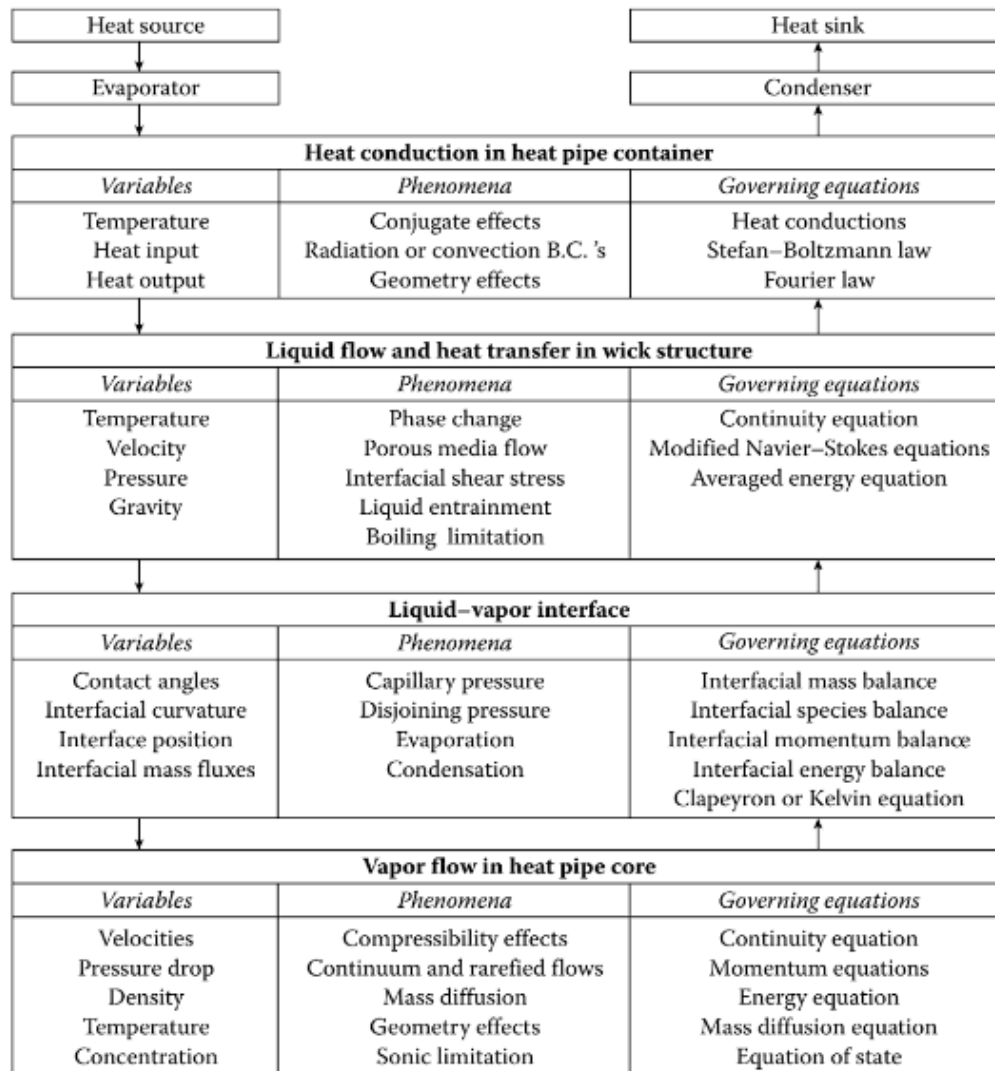| Variables	Phenomena	Governing equations
Velocities Pressure drop Density Temperature Concentration	Compressibility effects Continuum and rarefied flows Mass diffusion Geometry effects Sonic limitation	Continuity equation Momentum equations Energy equation Mass diffusion equation Equation of state

Figure 22: Heatpipe modelling. [5]

The variables included in the heatpipe model in this research are limited to the Temperature, Heat input and output, and pressure. The modelling of the heatpipe is simplified to heat flow in a resistance network.

4.2   The Resistance Model.

Steady state heat flow in the heatpipe is modelled as a resistance network analogous to an electrical network. Figure 23 gives a schematic drawing of a vertical heat pipe. From this figure a resistance model is derived shown in figure 24.
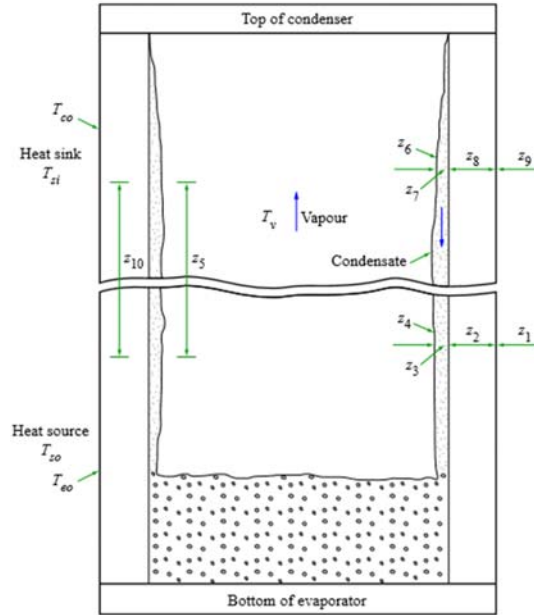

Figure 23: Schematic drawing of resistances in a heatpipe without wick structure. [7]
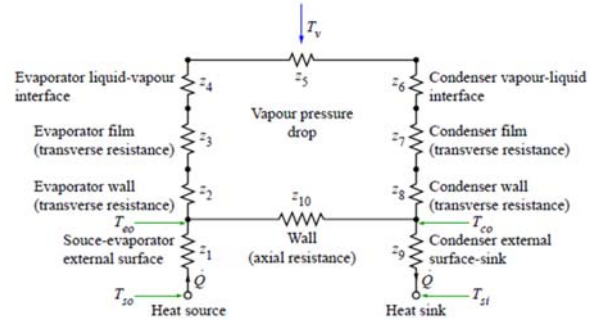
Figure 24: Heat flow resistance network for a heatpipe. [7]

The resistance to heat flow of the liquid and vapour depend on the fluid properties which in turn depend on the temperature. To account for the temperature dependency of the fluid properties the National Institute of Standards and Technology Refprop database [21] is used to evaluate these properties.

4.2.1   Simplifications.

To simplify the resistance network the order of magnitude of each of the resistances are compared using data from the VDI heat atlas [11] shown in table 3.

Resistance to heat flow	$\dfrac{K}{W}$
Wall radial resistance. z2, z8.	10^{-1}
Film and Capillary structure. z3, z7.	10^{+1}
Vapor liquid interface. z4, z6.	10^{-5}
Vapor axial resistance. z5.	10^{-8}
Wall axial resistance. z10.	10^{+2}
Film axial resistance.	10^{+4}

Table 3: Orders of magnitude of individual heat resistance. [34]

The resistance to axial heat conduction through the wall and the liquid film is expected to be at least ten orders of magnitude larger than the resistance of heat transport by vapour flow. Therefore, the heat flow through the wall and liquid film in the axial direction is neglected.

The resistance to radial heat conduction at the vapour liquid interface is expected to be at least 4 orders of magnitude smaller than the combined wall and film resistance. Therefore, the interface resistance is also neglected. Figure 25 shows the resulting simplified resistance network.
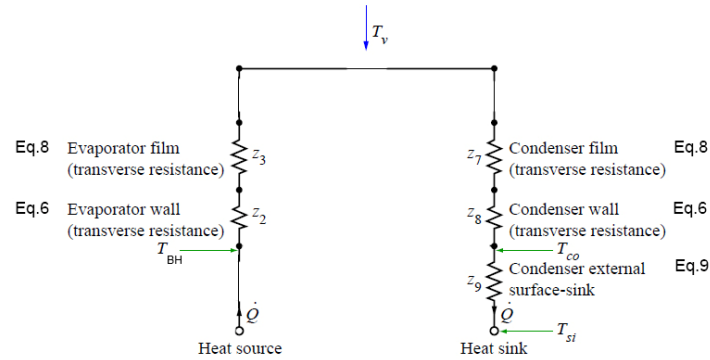

Figure 25: Simplified Heat Flow Resistance Network

4.2.2   Wall resistance

The wall heat flow resistance equation in cylindrical coordinates for the evaporator tube is defined with D_i, D_o the inner and outer tube diameter respectively as:

$$R_{Wall_{Evaporator}} = \frac{\ln\left(\frac{D_o}{D_i}\right)}{2 * \pi * l_e * k_w}$$

Equation 6: Conduction Resistance Cylinder [31]

Here k_w is the thermal conductivity of the wall material and l_e the total evaporator length.

4.2.3   Film resistance

The thermal resistance of boiling and condensing fluid are a function of the fluid properties, the dimensions and orientation of the heat pipe and the rate of heat transfer.

The thermal resistance of a film of condensate running down a smooth wall can be calculated with Nusselt's theory of film wise condensation [30, 31]. For a vertical tube, the film resistance in the condenser is defined as:

$$R_{Film_{Condenser}} = \frac{C_1 * \dot{Q}^{1/3}}{D_i^{\frac{4}{3}} * g^{\frac{1}{3}} * l_c * \phi_2^{\frac{4}{3}}}$$

Here C_1 is defined as $C_1 = \frac{1}{4} * \left(\frac{3}{\pi}\right)^{\frac{4}{3}} = 0.235$. $\dot{Q}$ is the heat flow and l_c is the total condenser length. The figure of merit ϕ_2 is defined in 2.3.1

The thermal resistance of the film in the evaporator under idealized conditions, i.e. just enough liquid and a smooth film in the whole of the evaporator, is the same in an evaporating film as in a condensing film [32]:

$$R_{Film_{Evaporator}} = \frac{C * \dot{Q}^{1/3}}{D_i^{\frac{4}{3}} * g^{\frac{1}{3}} * l_c * \phi_2^{\frac{4}{3}}}$$

ESDU 81038 [7] reports that in practice, it is often difficult to establish a smooth film of liquid on the inner surface of a pipe. Visual observations of ripples developing and the liquid film breaking up are reported in literature [14]. Experimental data has shown that the thermal resistance can be appreciably greater than predicted by Nusselt's film condensation theory when the film Reynolds number is below 50 [7]. At Reynolds numbers between 100 to 1300 Nusselt's Theory somewhat overestimates the thermal resistance [31] and above 1300 there is an appreciable fall in thermal resistance due to waves developing on the film and turbulence inside the film [31]. The Reynolds film number [7] is defined as:

$$Re_{film} = \frac{4 * \dot{Q}}{h_{fg} * \mu * l * \pi * D}$$

The following calculation scheme is advised by ESDU 81038 [7]. If there is a liquid pool in the evaporator the thermal resistance in the pool is given by the following correlation [32]:

$$R_{Pool} = \frac{1}{\phi_3 * g^{0.2} * \dot{Q}^{0.4} * (\pi * D * l_e)^{0.6}}$$

Where $\phi_3 = 0.32 * \frac{\rho_l^{0.65} * k^{0.3} * c_{pl}^{0.7}}{\rho_v^{0.25} * h_{fg}^{0.4} * \mu_l^{0.1}} * \left[\frac{p_v}{p_a}\right]^{0.23}$

The physical properties for the boiling figure of merit above are evaluated at atmospheric boiling temperature and the correlation has been shown to be valid for values of $\left[\frac{p_v}{p_a}\right]$ up to 20 [7].

If the film Reynolds number is above 1300 the following correction factor is applied to the resistance:

$$R_{pool} = R_{pool} * 191 * Re_f^{-0.733}$$

Equation 11: Pool-Boiling Correction Factor

The film resistance in the evaporator is calculated in the following manner with FR the fill ratio of the heatpipe.

$$if \ R_{Pool} < R_{Film} \ then \ R = R_{Pool}$$

$$otherwise \ interpolate \ using \ the \ fill \ ratio: \ R = R_{Pool} * FR + \ R_{Film} * (1 - FR)$$

The external resistance of the condenser zone of the heatpipe depends on the method used to remove the heat. In general if the heat transfer coefficient is known the resistance is given by:

$$R_{Condenser_{external}} = \frac{1}{h_{Condenser_{external}} * S_{Condenser}}$$

If the heat sink is a boiling liquid reference [31] is referred to for heat transfer correlations. In the case of natural convection reference [33] may be useful.

4.2.4   Heatpipe Model Sections
The heat pipe model is divided into sections. Each section uses the same underlying resistance model but differs in the correlations for resistance that are used. Heat transfer mechanisms in the pool and film section differ and are calculated by different correlations. There are four separate sections. The evaporator consists of two sections, one for the pool and one for the film region. The condenser and adiabatic part are each one section and the adiabatic part is assumed perfectly isolated.

4.2.5   Assumptions
The main assumption in the calculations for the heatpipe resistance is that the liquid and vapour are both at saturated equilibrium conditions. The consequence is that the temperature and pressure are no longer independent variables.

4.2.6   Calculation Scheme.
To start the calculations a first guess for the vapour temperature at the top of the condenser is based on the known external resistances. Figure 26 shows a typical profile of temperature in a heatpipe. The vapour temperature in the condenser is used to calculate the temperature at the bottom of the pool by calculating the hydrostatic head.

The heat flow resistance of the liquid film as well as the heat flow resistance in the pool depend on the heat flow and require iteration. The model that is implemented in MATLAB contains a while loop to reach convergence within a specified error margin. The same is implemented for the total heat flow through the heatpipe. The heat flow into the heatpipe and the heat flow out at the condenser have to be equal.

If the heat flows in and out are outside the specified error margin the vapour temperature will be adjusted and the calculation loop will run again. This process is repeated until the heat flows in and out are within the specified error margin, for the simulations run in this research the error margin is set to 25 Watt. Figure 27 gives a schematic block diagram of the calculation scheme that is implemented in MATLAB.
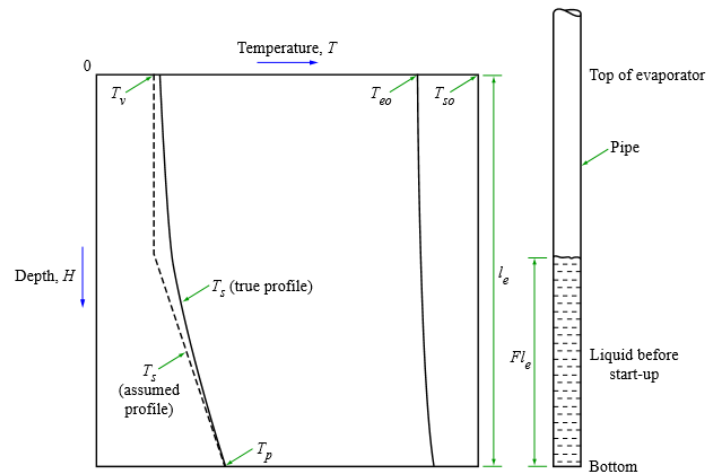

Figure 26: Typical Temperature Profile in a Heatpipe [7]

4.2.7   Model sensitivity.

The simplified resistance model takes into account the film, wall and external resistance. The wall resistance is a constant value that depends only on the material properties and the geometry. The material properties variation with temperature are very small [36] and neglected. The film resistance is dependendt on the fluid properties which vary significantly with temperature as well as the heat input. Thus at a constant heat input the sensitivity is dictated by the variation of the fluid properties. The experiments in this research are varied between 40 to $60°C$. The variation in heat transfer coefficient calculated in this research gives a difference of about 11% between $40°C$ and $60°C$.
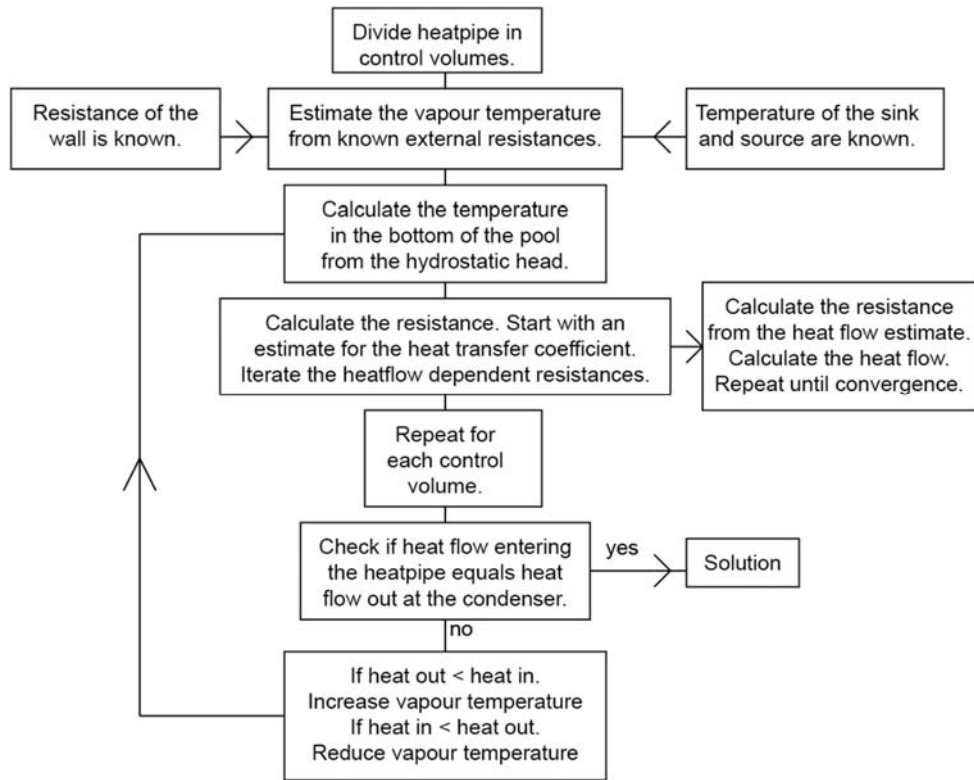
Figure 27: Block diagram calculation scheme.

5   Results & Conclusions

5.1 Summary of results

The results show data collected from seven experiments ranging from $493W$ to $1960W$ input. Figure 28 shows the heat leaving the system through the plate heat exchanger. The figure shows that the heat flow through the system from the start of experiments increases until it reaches a nearly steady value.
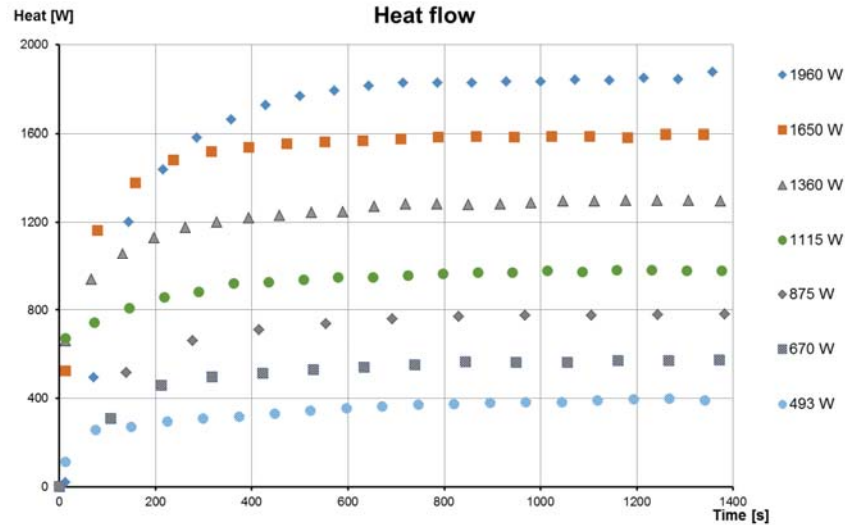

Figure 28: Heat flow out at the condenser versus time.

Figure 29 shows the efficiency of the system over time. The efficiency is defined as the measured heat output at the condenser compared to the electrical input at the evaporator and given in equation 12. The figure shows the start-up time of the heatpipe and it shows that for a larger heat flow the efficiency increases. The larger heat flows appear to converge to a value of about 95% efficiency.

$$Efficiency = \left(1 - \frac{(\dot{Q}_{in} - \dot{Q}_{out})}{\dot{Q}_{in}}\right) * 100\%$$

Equation 12: Efficiency
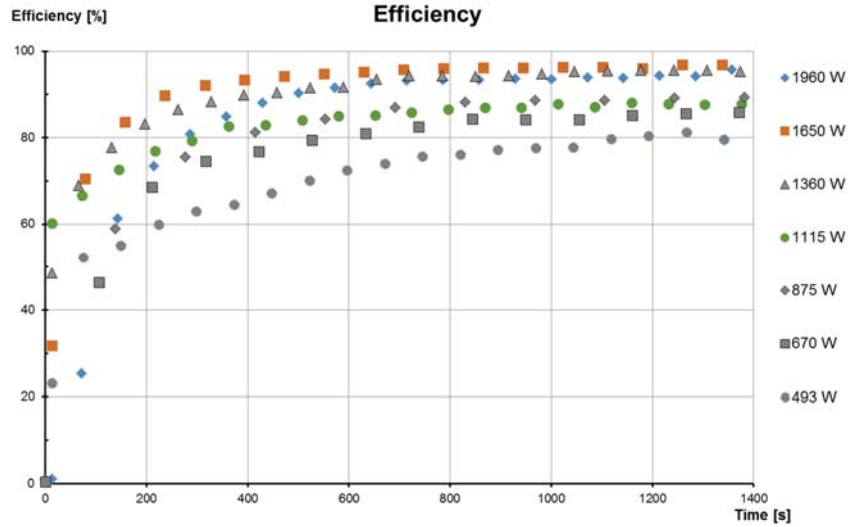
Figure 29: Efficiency of heat transport.

Figure 30 shows the resistance to heat transfer of the evaporator defined in equation 13. The figure shows the resistance quickly reaches a near constant value. The figure shows a general trend where larger heat input values show lower heat flow resistance. It also shows that the difference in resistance decreases with increasing heat flow. The larger heat flows appear to converge to a resistance value of about $0.022 \frac{K}{W}$.

$$Resistance_{evaporator} = \frac{\Delta T}{\dot{Q}}$$

Equation 13: Resistance evaporator.
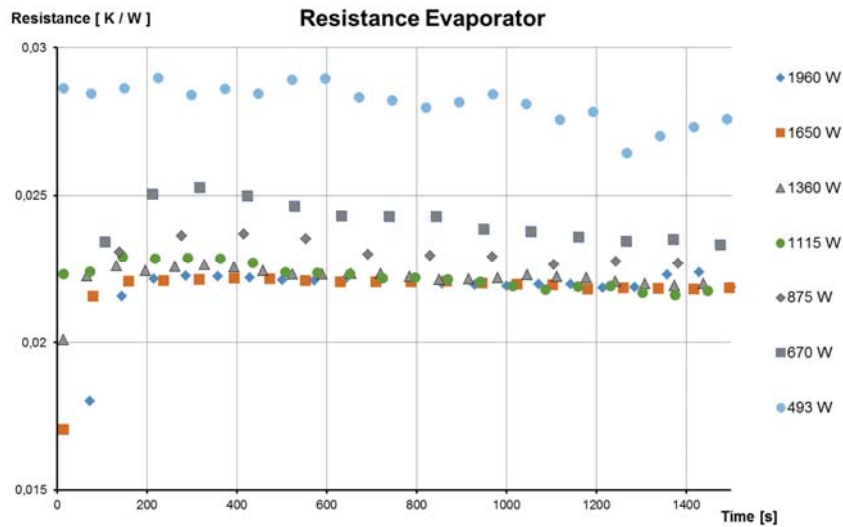
Figure 30: Heat Flow Resistance Evaporator.

Figure 31 shows the resistance to heat flow over the condenser defined in equation 14. The figure shows that the resistance of the condenser is constantly increasing with time. It also shows a trend of lower resistance to heat flow for larger heat input values similar to the evaporator.

$$Resistance_{condenser} = \frac{\Delta T}{\dot{Q}}$$

Equation 14: Resistance condenser.

Figure 31: Heat Flow Resistance Condenser.

5.2 Discussion

In this paragraph the experimental and model results are compared. The theoretical model is supplied with data for the average evaporator and condenser temperature as well as the condenser resistance as input. The model does not calculate the resistance over the condense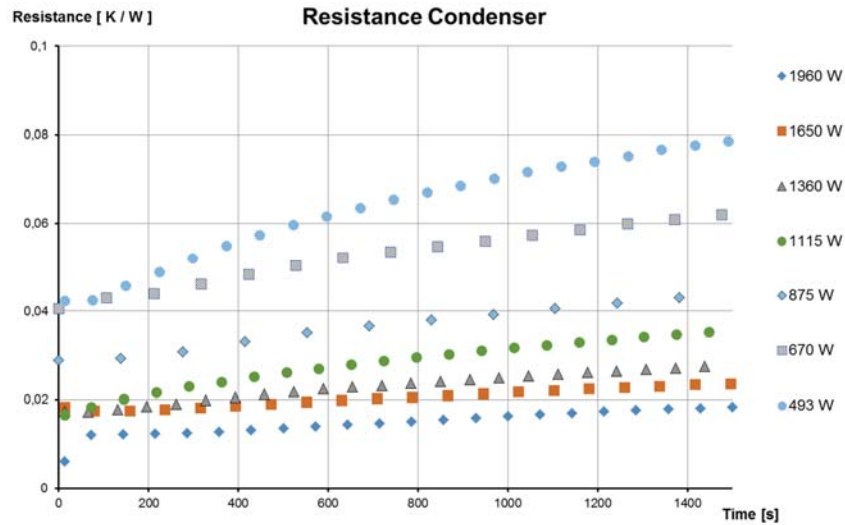r. The reason is that in experiments the condenser resistance was significantly higher than expected from theory. This is presumably due to air leakage into the prototype and subsequent air bubbles forming in the condenser that deteriorate heat transfer. The model does not contain any heat losses to the environment or to the thermal mass of the system

Heat flow in and out of the heatpipe set-up.

In figure 32 the measured heat flow at the condenser is plotted against the heat input. The heat in and output is showing a near constant offset. The average difference between the heat input and output is about 105 Watt. This difference can largely be explained by heat loss.
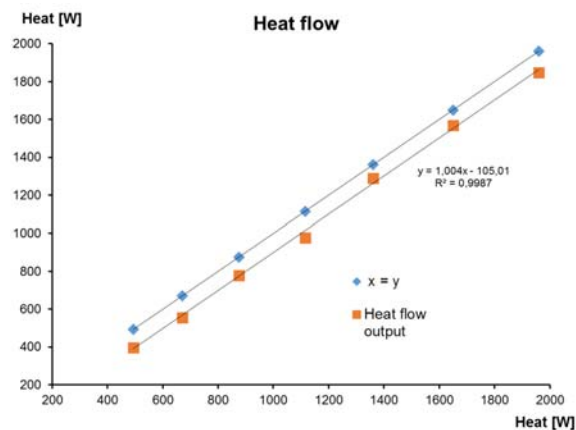
Figure 32: Heat input vs heat output.

Table 4 shows averaged data for the heat flow input and output.

Heat flow input [W]	Heat flow output [W]	Difference [W]	Average Efficiency [%]
1960	1849	111	94.3
1650	1568	82	95
1360	1290	70	94.9
1115	976	139	87.5
875	778	97	88.9
670	555	115	82.8
493	396	97	80.3

Table 4: Heat flow in vs Heat flow out.

To estimate heat loss the heatpipe is modelled as two parts. The first part consists of the band heaters surrounded with insulation where the temperature of the heaters is measured and the outside temperature of the insulation is at the ambient temperature of $20°C$. The second part is the heatpipe adiabatic section with known operating temperature. The temperature difference over the adiabatic section is taken as the difference between the fluid temperature and the ambient temperature. For both parts, the combined convective and radiative heat flow resistance to the environment is neglected.

According to Mills [37] the magnitude of the convective heat transfer coefficient for natural convection is in the order of 3 to 25 $\frac{W}{m^2K}$ which by itself is at least two orders of magnitude larger than the conduction resistance of the insulation.

The thermal conduction coefficient of Plexiglas is $0.2\frac{W}{m^2K}$, the insulation conduction coefficient is $0.04\frac{W}{m^2K}$. The thickness of the Plexiglas is 4 mm, the thickness of the insulation is 12 mm. The Fourier equation in cylindrical coordinates is used to estimate the heat loss.

$$R_{BandHeaters} = * \frac{\ln\left(\frac{r_o}{r_i}\right)}{2 * \pi * L_{BH} * k_{Insulation}}$$

$$Q_{loss,BandHeaters} = \frac{\Delta T}{R_{BandHeaters}} = 13 \ W \ at \ 100°C$$

$$R_{Adiabatic} = \frac{\ln\left(\frac{r_o}{r_i}\right)}{2 * \pi * L_{Adiabatic} * k_{Insulation}} + \frac{\ln\left(\frac{r_o}{r_i}\right)}{2 * \pi * L_{Adiabatic} * k_{Plexiglas}}$$

$$Q_{loss,Adiabatic} = \frac{\Delta T}{R_{Adiabatic}} = 50 \ W \ at \ 60°C$$

$$Q_{loss,total} \cong 63 \ W$$

The calculated heat loss does not take into account any heat that goes towards the thermal mass of the systems and the assumed model geometry is simplified as heat loss at the connections to the condenser and the condenser itself are neglected. The total surface where heat loss can occur is underestimated.

Although the heat loss approximation of 63 Watt is simplified, the order of magnitude matches with the heat loss that is expected from the experimental data. For the range of heat input in experiments, this is a significant loss and it shows the importance of insulation especially for longer heatpipes.

Resistance to heat transfer of the evaporator.

Figure 33 shows the resistance to heat flow over the evaporator as a function of the heat flux. The experimental data shows that for increasing heat flux the resistance to heat flow decreases. To investigate the resistance associated with boiling a corrected resistance is calculated by subtracting the conduction resistance of the evaporator tube. The resistance is defined in equation 15 and obtained from data of the average temperature difference and the heat input.

$$Resistance_{evaporator} = A\frac{\Delta \bar{T}}{\dot{Q}_{in}}$$
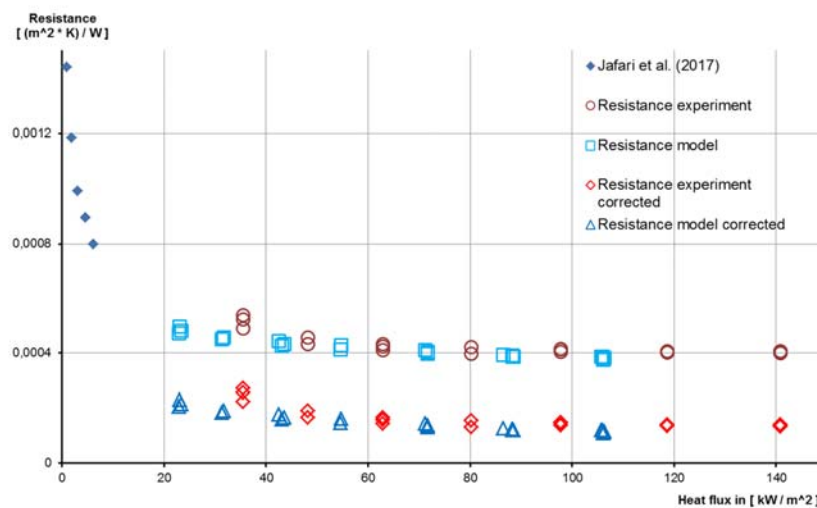
Figure 33: Resistance Evaporator vs Heat Input

Figure 33 includes resistance data from Jafari [10]. Jafari performed experiments with a thermosiphon constructed from a one millimetre thin walled copper tube. The data from Jafari, although outside the range of the experimental data, shows a similar trend where the heat transfer resistance decreases with increasing heat flux.

Nucleate boiling.

Several correlations are available for predicting the heat transfer coefficient associated with nucleate boiling. Rohsenow (1952) was the first to propose a correlation for boiling heat transfer based on the argument that heat transfer enhancement under boiling is the result of local liquid circulation in the region close to the heating surface promoted by successive bubble detachment. The correlation proposed by Rohsenow [24] is given in equation 16. The correlation is based on the mass velocity of vapour leaving the surface and a characteristic dimensional length proportional to the bubble departure length. The numerical coefficient C_{sf} is related to the contact angle.

$$St^{-1} = C_{sf} * Re_b^m * \Pr_l^n$$

Rohsenow initially proposed constant values for the exponents n and m for all fluid-surface combinations. The values of n and m have since been researched for many fluid-surface combinations and values are available in literature.

A recent study by Jafari et. al. [10] into evaporation heat transfer correlations for thermosiphons concluded that a correlation by Imura et. al. [34] gave the best results for vertical thermosiphons with a fill ratio between 50 to 100% and a high heat flux. No clear definition was given of what constitutes a high heat flux.

$$h_{e,p} = 0.32 \left(\frac{\rho_l^{0.65} * k_l^{0.3} * C_{p,l}^{0.7} * g^{0.2}}{\rho_v^{0.25} * h_{fg}^{0.4} * \mu_l^{0.1}} \right) \left(\frac{p_v}{P_{atm}} \right)^{0.3} * q^{0.4}$$

Figure 34 shows the heat transfer coefficients measured in the experiment as well as predicted by the model. The correlations proposed by Imura [34] and Rohsenow [24] are the long green and short red dashed lines respectively.
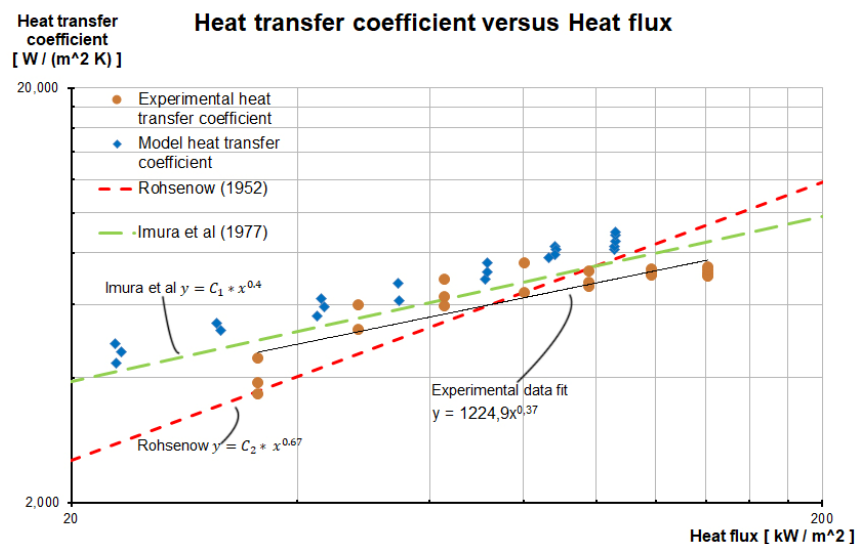

Figure 34: Heat transfer coefficient versus heat flux.

Figure 35 compares the measurements with both correlations and data from literature [35, 36]. Boiling heat transfer is difficult to predict accurately due to the influence of parameters such as those related to the geometry and orientation. The proposed correlation by Imura et. al. shows a good fit to the measurements. The correlation dictates a relationship between the heat transfer coefficient and the heat flux of $q^{0.4}$. The measurement data shows a growth rate with $q^{0.37}$. Both the magnitude and the exponential increase of the heat transfer coefficient with increased heat flux for the measurements shows a good match to the correlation. The model implements this correlation for the pool boiling heat transfer coefficient. The offset between the model data points and the correlation is due to a varying temperature. The correlation is displayed for $40°C$.
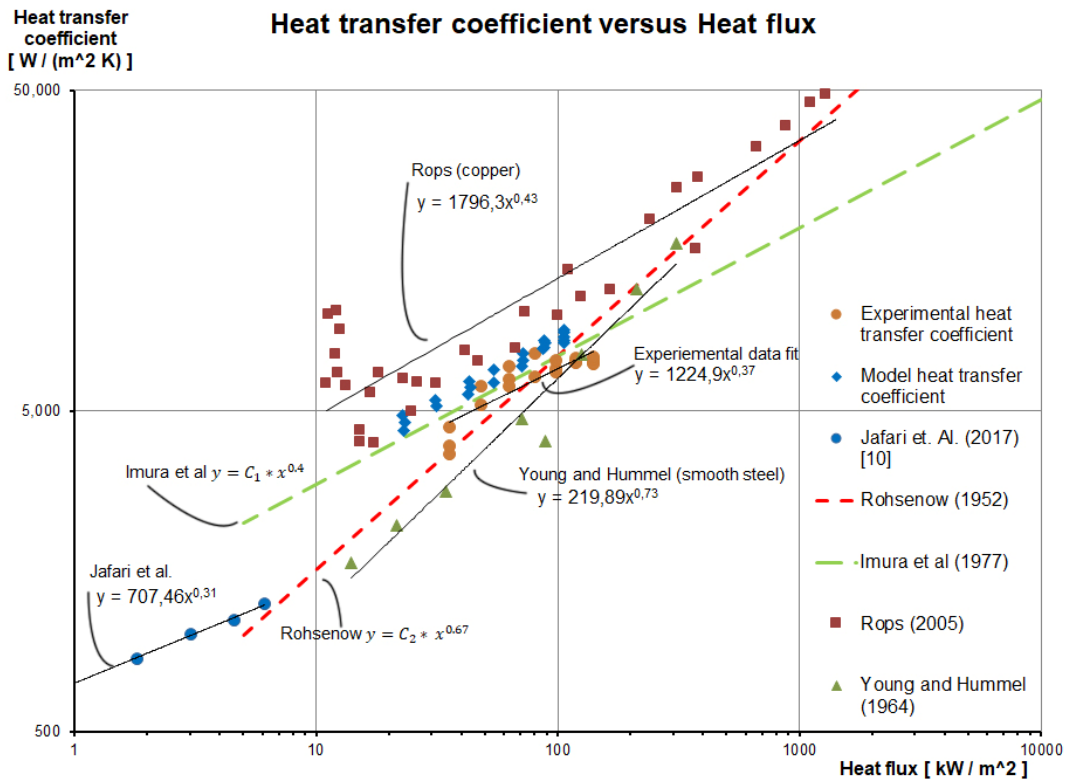

Figure 35: Heat transfer coefficient versus heat flux.

The measurements from Jafari et. Al. [10] show a slower growth with $q^{0.3}$ as is expected from the general boiling curve shown in figure 8. The measurements are about a decade lower in heat flux on the boiling curve where the enhanced heat transfer associated with the change from natural convection to nucleate boiling is increasing.

5.3 Conclusions and recommendations.

Heat flow.

It is found that the difference in heat flow input and output is largely explained by a heat loss of about $100W$ to the environment. This also explains the increase in efficiency at larger heat flows as this heat loss is a smaller fraction of the total heat flow.

The heatpipe set up has a heat loss of about 100 W to the environment. This is between 5 and 20% of the total heat flow for 2 kW and 500W heat input respectively. For a geothermal heatpipe the heat loss to the environment is expected to scale linearly with the length of the adiabatic section. Depending on the temperature in the heatpipe for long heatpipes insulation of a portion of the heatpipe can be important.

Heat transfer coefficient.

Results show the heat transfer coefficient for boiling can be modelled using the proposed correlation by Imura. Both the magnitude and the exponential increase of the heat transfer coefficient with increased heat flux is predicted very well for a fill ratio of 100%.

Leakage.

The condenser resistance is not investigated in this research. Due to air leakage into the system measurement data for the condenser is deemed unusable. The reason is that the amount of air in the system is unknown and is likely different between tests.

The performance of the heatpipe is affected by the amount of non-condensable gasses in the system. When air is leaking into the system the heatpipe behaviour over time will move away from the initial steady state and the heatpipe temperature will increase to compensate for the increasing resistance to heat flow on the condensing side of the heatpipe. This will continue until the air reaches a critical amount after which the heatpipe performance quickly deteriorates.

Repeatability experiments.

Due to air leakage into the system repeatability of the experiments was a concern. To check repeatability several experiments were repeated with three days between the experiments. The repeatability experiments however showed a near exact match in both efficiency and evaporator resistance. The condenser resistance showed equal but time shifted behaviour, which is assumed to be due to variance of the amount of air that leaked into the system.

Current set-up.

The experiments showed that measurements can be performed on the evaporating side of the heatpipe. However to do measurements at a true steady state more testing should be done to find and fix the air leakage into the system. The heatpipe set-up is constructed to handle a heating load of 10 kW. Experiments can be performed at larger heat flows to further investigate the heatpipe limits and the accuracy of the predictions from theory.

Fill Ratio.

All experiments with the heatpipe set-up used a fill ratio of 100%. Literature shows that lower fill ratios can improve the overall heat transfer coefficient as shown in figure 36 [39]. There is a limit to lowering the fill ratio that depends on the heat input that is caused by dry-out [38, 39]. For a geothermal heatpipe a large pool is not an option due to the hydrostatic pressure in the pool. This means that for long evaporation sections the heatpipe will have to operate with an amount of liquid that is just enough to create a continuous film but without creating a large pool. As of yet the author has found no literature for predicting the optimal fill ratio and dry-out in literature neither from numerical predictions nor from experimental correlations. Therefore investigating the required fill ratio and the limit due to dry-out is important for a potential geothermal heatpipe.
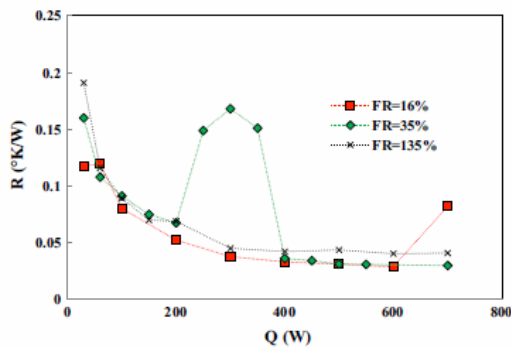
Figure 36: Overall heat transfer resistance as a function of heat input for different fill ratios.
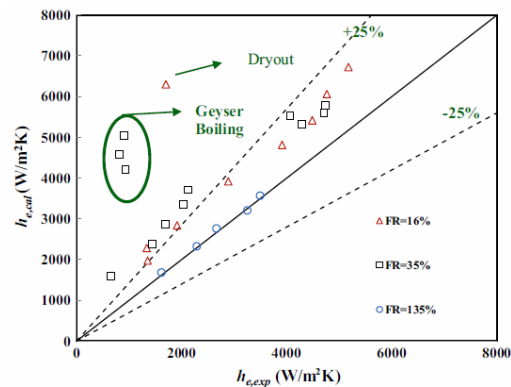
Figure 37: Predicted (Imura correlation) versus experimental heat transfer coefficient evaporator.

Future set up.

For a geothermal heatpipe the pressure/temperature drop over the heatpipe itself may play an important role in the design and limitations of a geothermal heatpipe. The evaporator section of a long geothermal heatpipe should be researched further as it is thought to be the limiting section of the heatpipe. For a future set-up the author would recommend a set-up consisting of mainly an evaporator section where it is possible to gain more insight into the fluid flow along the heatpipe, the pressure and temperature drop over the length and limitations to the amount of liquid in the heatpipe.

Fluid flow in the heatpipe.

Observations during operation of the heatpipe showed that liquid on the the pipe circumference did not behave like an ideal film. The condensate formed thick streaks of liquid flowing in a pulsing behaviour in what appeared to be random paths. It is expected that for a geothermal heatpipe which has a very large evaporator surface that wetting of this surface is important and perhaps the limiting mechanism in heat transfer performance. Therefore reseach into requirements and limitations to this film flow is recommended.

Economic viability and practical challenges.

A geothermal heatpipe is an interesting concept as it is at the top of efficient heating technologies. One of the main challenges will be in providing systems that are economically viable.

Several practical challenges remain such as the high hydrostatic pressure in deep soil and ground-water layers. A solution could be to match the fluid inside the heatpipe to operate at a high vapour pressure that is similar to the surrounding pressure such that the heatpipe walls do not require excess thickness. However for very long heatpipes this might then require multiple heatpipe sections with different fluids which brings new practical challenges as well as a reduced economic viability.

6 Appendix

6.1 Prototype heatpipe parameters

	Evaporator tube	Adiabatic tube
Length	0.139 m	1.5 m
ID	54.76 mm	52 mm
OD	60.3 mm	60 mm
Fill Ratio	1	
Power input	2 x 1000 W	

6.2 Parts and Materials

6.2.1 Band heaters.

Attached to the evaporator tube are two $1000\ W$ watlow band heaters. The heaters are clamped on the tube with two bolts that pull the heater around the tube.

The heated area of the band heaters is approximated using the suggested formula and "no-heat factor" from the manufacturer.

This heated area is used to calculate a shape factor in radials to correct the heated area of the evaporator tube that is used in heat flow and resistance calculations.

$$\dot{Q} = \frac{S_f}{Resistance} * \Delta T$$

$$Resistance = \ln\left(\frac{D_o}{D_i}\right) * (2 * \pi * k_w * L)^{-1}$$

$$S_f = \frac{\Theta_{heated}}{2 * \pi}$$

Type	No-Heat Factor in.
1 pc. lead unit Type B, C, H, E or 90°B	1.37
1 pc. post terminal	1.60
1 pc. expandable post term	3.18
1 pc. expandable lead unit	3.00
True 2 pc. post term	3.20
True 2 pc. leads	2.74
SLE	3.68

. To use the formula below, insert the no-heat factors, diameter and width (in inches).

Heated Area =
(3.14 x Diameter - No-Heat Factor) x Width

Figure 38: Watlow heater catalogue.

6.2.2 Evaporator.

The evaporator zone is a stainless steel 310 tube, shown in figure 16, with an outer diameter of $60.3\ mm$ and $2.77\ mm$ thickness. The length of the tube is 0.5 meter with a stainless steel flange welded at the top end. The bottom end is closed with a Plexiglas cap secured and sealed with a Viton O-ring.

Figure 39: The Evaporator Tube

Figure 40: Plexiglas Flange with red O-ring

Figure 41: Plate Heat Exchanger

6.2.3 Adiabatic section Plexiglas tube

The Adiabatic section consists of a Plexiglas tube that has a specially turned connection flange, shown above in figure 17, to connect to the stainless steel evaporator tube flange. The flange has been turned on a lathe to have a conically shaped internal diameter to create a smooth wall between the inside diameter of the Plexiglas tube and the inside diameter of the stainless steel tube.

6.2.4 PVC t-piece

A PVC T-piece with a $45°$ bend at the top of the Plexiglas tube allows for a top viewing window as well as directing the steam flow to the condenser. PVC pipes connect the PVC T-piece and the condenser. The connection piece consists of two rings that thread into each other with an O-ring for sealing. The other PVC pieces are glued.

6.2.5 Plate heat exchanger

The condenser is a commercially available soldered 304 stainless steel plate heat exchanger shown in figure 18. The heat exchanger has 10 plates with a total area of approximately $0,12 \ m^2$. The dimensions are available in Appendix 6.1.2.

6.2.6 Insulation

For insulating the heatpipe set-up armacell foam is used. This flexible foam is supplied in tube sections of different diameters measuring about 12 mm in thickness. Specifications can be found in appendix 6.1.

6.2.7 Electrical System

The heaters are powered with a variable current power supply. The voltage can be set to a value between zero and 240 V. This corresponds to regulating the power to the band heaters from zero to 2 kW.

6.2.8 Cooling circuit with recirculation bypass

The cooling circuit is integrated in the building delivering a water flow between a constant 13 to 15 $°C$. To vary the temperature at the inlet of the condenser a bypass circuit has been added over the condenser. This circuit consists of a pump connecting the inlet and outlet of the condenser to recirculate a fraction of the heated return flow.

6.2.9 Armaflex Insulation

Thermal conduction values $k_{insulation}$ in $\frac{W}{m*K}$ as a function of temperature in $°C$ are in table 5. The insulation thickness used on the prototype is 12 mm.

Thermal Conductivity at 0°C	0.034 W/(m · K)	
Thermal Conductivity at +20°C	0.036 W/(m · K)	Test acc. to EN ISO 8497
Thermal Conductivity at +40°C	0.038 W/(m · K)	

Table 5: Armacell k values for different temperatures

6.2.10 Plate Heat Exchanger dimensions

Figure XX below shows the dimensions for plate heat exchanger used in the heatpipe prototype. The heat exchanger model is B3-12A-10-2.0. The heat exchanger is rated for heat up to 22 kW and 20 bar pressure.
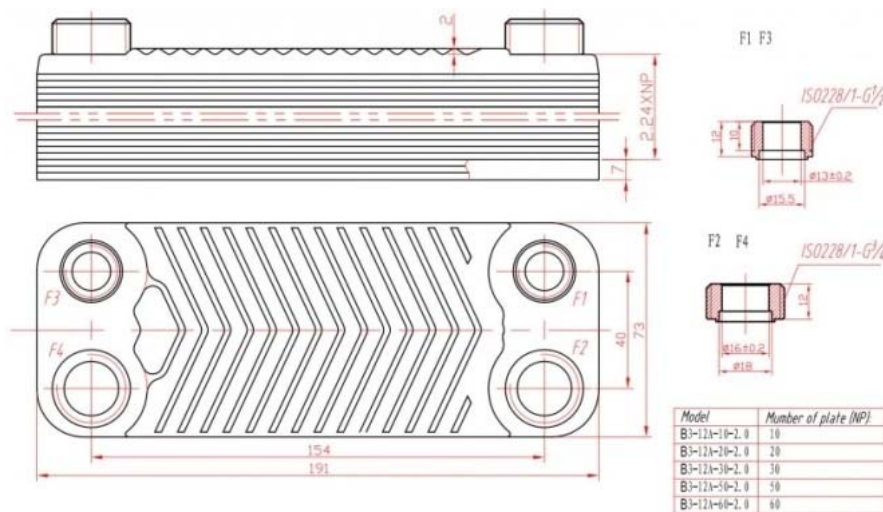
6.3 Working Fluid

6.3.1 Common fluids and their useful operating range

The useful range for the fluids in table 6 below extends from a minimum vapour pressure of 0.1 to 20 bar.

Working Fluid	Melting Point, K at 1 atm	Boiling Point, K at 1 atm	Useful Range, K
Helium	1.0	4.21	2-4
Hydrogen	13.8	20.38	14-31
Neon	24.4	27.09	27-37
Nitrogen	63.1	77.35	70-103
Argon	83.9	87.29	84-116
Oxygen	54.7	90.18	73-119
Methane	90.6	111.4	91-150
Krypton	115.8	119.7	116-160
Ethane	89.9	184.6	150-240
Freon 22	113.1	232.2	193-297
Ammonia	195.5	239.9	213-373
Freon 21	138.1	282.0	233-360
Freon 11	162.1	296.8	233-393
Pentane	143.1	309.2	253-393
Freon 113	236.5	320.8	263-373
Acetone	180.0	329.4	273-393
Methanol	175.1	337.8	283-403
Flutec PP2	223.1	349.1	283-433
Ethanol	158.7	351.5	273-403
Heptane	182.5	371.5	273-423
Water	273.1	373.1	303-550
Toluene	178.1	383.7	323-473
Flutec PP9	203.1	433.1	273-498
Naphthalene	353.4	490	408-623
Dowtherm	285.1	527.0	423-668
Mercury	234.2	630.1	523-923
Sulphur	385.9	717.8	530-947
Cesium	301.6	943.0	723-1173
Rubidium	312.7	959.2	800-1275
Potassium	336.4	1032	773-1273
Sodium	371.0	1151	873-1473
Lithium	453.7	1615	1273-2073
Calcium	1112	1762	1400-2100
Lead	600.6	2013	1670-2200
Indium	429.7	2353	2000-3000
Silver	1234	2485	2073-2573

Table 6: Common fluids and their useful operating range ordered from low to high temperature. [5]

6.3.2   Material compatibility

Table 7 shows compatibility between common container materials and working fluids.

Working Fluid	Compatible Material	Incompatible Material
Water	Stainless Steel[a], Copper, Silica, Nickel, Titanium	Aluminum, Inconel
Ammonia	Aluminum, Stainless Steel, Cold Rolled Steel, Iron, Nickel	
Methanol	Stainless Steel, Iron, Copper, Brass, Silica, Nickel	Aluminum
Acetone	Aluminum, Stainless Steel, Copper, Brass, Silica	
Freon-11	Aluminum	
Freon-21	Aluminum, Iron	
Freon-113	Aluminum	
Heptane	Aluminum	
Dowtherm	Stainless Steel, Copper, Silica	
Lithium	Tungsten, Tantalum, Molybdenum, Niobium	Stainless Steel, Nickel, Inconel, Titanium
Sodium	Stainless Steel, Nickel, Inconel, Niobium	Titanium
Cesium	Titanium, Niobium, Stainless Steel, Nickel-based superalloys	
Mercury	Stainless Steel[b]	Molybdenum, Nickel, Tantalum, Inconel, Titanium, Niobium
Lead	Tungsten, Tantalum	Stainless Steel, Nickel, Inconel, Titanium, Niobium
Silver	Tungsten, Tantalum	Rhenium

[a]Sensitive to cleaning; [b]with Austenitic SS

Table 7: Material Compatibility [5]

7   References

1. *Gaugler, R. S. (1944)*
Heat transfer device . U.S. Patent 2,350,348.
2. *Trefethen, L. (1962)*
On the surface tension pumping of liquids or a possible role of the candlewick in space exploration . G. E. Tech. Info., Ser. No. 615 D114.
3. *Wyatt, (1963)*
Satellite temperature stabilization system. Early development of spacecraft heat pipes for temperature stabilization. (Johns Hopkins/Applied Physics Lab) U.S. Patent No. 3,152,774.
4. *Grover, G., Cotter, T. and Erickson, G. (1964)*
Structures of Very High Thermal Conductance. Journal of Applied Physics, 35(6), pp.1990-1991.
5. *Faghri, A. (2014)*
Heatpipes: Review, opportunities and challenges. Frontiers in Heat Pipes. DOI:10.5098/fhp.5.1.
6. *ESDU 80017 (1980)*
Heat pipes – performance of two-phase closed thermosyphons.
7. *ESDU 81038 (1981)*
Heatpipes performance of capillary driven designs.
8. *ESDU 810017 (1980)*
Thermophysical properties of heat pipe working fluids.
9. *Larkin, B.S. (1981)*
An experimental study of the temperature profiles and heat transfer coefficients in a heat pipe for a heat exchanger. Advances in Heat Pipe Technology: IV International Heat Pipe Conference, London, Pergamon Press, Oxford.
10. *Jafari et al. (2017)*
An experimental investigation on the evaporation and condensation heat transfer of two phase closed thermosiphons. University of Twente.
11. *Bezrodnyi, M.K. et all (1982)*
Study of hydrodynamic characteristics of two-phase flow in closed thermosyphons. Advances in Heat Pipe Technology: IV International Heat Pipe Conference, London, September 1981. Pergamon Press, Oxford.
12. *VDI HEAT ATLAS (1993)*
N5 Heatpipes. Second edition. Springer.
13. *Andrew Smith. (March 1990)*
A preliminary investigation into the geothermal application of long heatpipes. Canterbury, UK.
14. *Geoscience Australia [online]*
Available at: https://www.ga.gov.au/scientific-topics/energy/resources/geothermal-energy-resources - [Accessed 03-12-2018].
15. *Kundu P. K. et all. (1990)*
Fluid mechanics. Elsevier Science. Academic Press.
16. *Muthu, V. et all. (2017)*
Embedded thermal management solution for power electronics PCB using additive manufacturing. Asian Conference on Energy, Power and Transportation Electrification.
17. *Faghri, A. (1995)*
Heat Pipe Science and Technology, 1st ed., Taylor & Francis, Washington, D.C.
18. *Engineering ToolBox. (2003) [online]*
Thermal Conductivity of common Materials and Gases. Available at: https://www.engineeringtoolbox.com/thermal-conductivity-d_429.html [Accessed 06-12-2018].
19. *Engineering ToolBox. (2003) [online]*

Water - Thermophysical Properties. Available at: https://www.engineeringtoolbox.com/water-thermal-properties-d_162.html [Accessed 06-12-2018].

20. Engel. Y. A. C. (1998)
Heat Transfer: A Particle Approach (2nd ed.) ch 10, pp. 518–519, McGraw-Hill.

21. NIST REFPROP. (2010)
National Institute of Standards and Technology, Reference Fluid Thermodynamic and Transport Properties, Database 23, Version 9.0.

22. Zijm, P. (2017)
Evaluating several types of downhole heat exchangers for the extraction of geothermal heat from abandoned oil and gas wells. (Internship TNO as part of the TU Delft master program).

23. Kerlin, Thomas W. and Shepard, Robert L. (1982)
Industrial Temperature Measurement. s.l. Instrument Society of America.

24. Rohsenow, W. M., (1952)
A Method of Correlating Heat Transfer Data for Surface Boiling Liquids. Transactions of ASME, Vol.74, pp. 969-976.

25. Peters, S. M. (2011)
Thermocouple Temperature Measurements for Twin Jet Thermal Mixing. University of Tennessee.https://trace.tennessee.edu/utk_gr adthes/1090.

26. National Instrutments (2016) [online]
Thermocouple basics – http://www.ni.com/white-paper/53184/en/. [Accessed 06-12-2018].

27. Omega Engineering inc. [online]
https://www.omega.com/techref/ThermocoupleResponseTime.html. [Accessed 06-12-2018].

28. RS-PRO RS 409 – 4908 DATA SHEET [online]
RS 409 – 4908 (PTFE) THERMOCOUPLE SENSOR https://docs-emea.rs-online.com/webdocs/157a/0900766b8157a377.pdf [Accessed 06-12-2018].

29. Kern, D.Q. (1950)
Process heat transfer. McGraw-Hill.

30. Mc Adams, W.H. (1954)
Heat transmission, 3rd Edition. McGraw-Hill.

31. Shiraishi, M. et al. (1981)
Investigation of heat transfer characteristics of a two-phase closed thermosyphon. Advances in Heat Pipe Technology: IV International Heat Pipe Conference, London. Pergamon Press, Oxford, 1982.

32. ESDU 77031 (1977)
Heat transfer by free convection and radiation–simply shaped bodies in air and other fluids. International plc, London.

33. H. Imura, H. Kusada, J. Oyata, T. Miyazaki, N. Sakamoto. (1977)
Heat transfer in two phase closed-type thermosiphons, Trans. Japan. Soc. Mech. Eng. 22 485–493.

34. Rops, C.M., Lindken, R., Westerweel, J., and Velthuis, J.F.M. (2005)
Enhanced heat transfer for pool boiling at microscale. ECI International conference on heat transfer and fluid flow in microscale, Castelvecchio Pascoli, Italy.

35. Young, R.K., and Hummel, R.L. (1964)
Improved nucleate boiling heat transfer. Chemical engineering progress, 60(7) pp. 54-58.

36. Asselman G.A.A, Green D.B. (1973)
Heat pipes. Philips Techn Rev 33:104-113

37. Mills, A.F. (1999)
Basic Heat and Mass Transfer. Second edition. Prentice hall.

38. Shabgard, H. et all (2013)
Thermal characteristics of a closed thermosyphon under various filling Conditions. International Journal of Heat and Mass Transfer.

39. Jafari, D. Filippeschi, S. Franco, A. Di Marco, P. (2017)
Unsteady experimental and numerical analysis of a two-phase closed thermosyphon at different filling ratios. Experimental Thermal and Fluid Science.